Analysis of underground concrete pipelines subjected to seismic high-frequency loads

Roghayeh Abbasiverki

Licentiate Thesis in Civil and Architectural Engineering

Concrete Structures

KTH Royal Institute of Technology

Stockholm, Sweden, 2016

TRITA-BKN. Bulletin 138, 2016
ISSN 1103-4270
ISRN KTH/BKN/B--138--SE

Abstract

Buried pipelines are tubular structures that are used for transportation of important liquid materials and gas in order to provide safety for human life. Such infrastructure systems crosses large areas with different geological conditions. During an earthquake, imposed loads from soil deformations on concrete pipelines may cause severe damages, possibly causing disturbance in vital systems, such as cooling of nuclear power facilities. The high level of safety has caused a demand for reliable seismic analyses, also for structures built in the regions that have not traditionally been considered as highly seismically active. The focus in this study is on areas with seismic and geological conditions corresponding to those in Sweden and Northern Europe. Earthquakes in Sweden are classified as intraplate events which for regions with hard rock may result in earthquakes dominated by high-frequency ground vibrations. Propagation of such high-frequency waves through the rock mass and soil medium affect underground structures such as pipelines.

The aim of this project is investigating parameters that affect response of buried pipelines due to high-frequency seismic excitations. The main focus of the study is on reinforced concrete pipelines. Steel pipelines are also studied for comparison purposes. Two-dimensional finite element models are developed for dynamic analysis of pipelines loaded by seismic waves that propagate from the bedrock through the soil. The models describe both longitudinal and transverse cross-sections of pipelines. The interaction between pipelines and surrounding soils is accounted for, including a nonlinear behaviour. The pipelines studied are assumed to be surrounded by frictional soils with dense, medium and loose stiffness. The effects of water mass, burial depth, soil layer thickness and non-uniform ground thickness caused by inclined bedrock are studied. It is demonstrated how two-dimensional plane strain models can be used for seismic analysis of pipelines with circular cross-sections.

The results are compared to those obtained for low-frequency earthquakes and the relationship between strong ground motion parameters and pipelines response is investigated. It is shown that the natural frequency of the models significantly depends on the soil type, soil layer thickness and non-uniformity of the ground. It is shown that, especially for high frequency earthquake excitations, non-uniform ground thickness due to inclined bedrock significantly increase stresses in the pipelines. For the conditions studied, it is clear that high-frequency seismic excitation is less likely to cause damage to buried concrete pipelines. However, the main conclusion is that seismic analysis is motivated also for pipelines in high-frequency earthquake areas since local variation in the ground conditions can have a significant effect on the safety.

Keywords: Earthquake, High-frequency, Underground, Pipelines, Reinforced concrete, Inclined bedrock.

Sammanfattning

Nedgrävda rörledningar (pipelines) är rörformiga strukturer som används för transport av viktiga flytande material och gas för att säkerhetsställa samhälleliga funktioner. Denna typ av infrastruktursystem korsar stora områden med olika geologiska förhållanden. Under en jordbävning kan markdeformationer påverka rörledningar av betong vilka kan få allvarliga skador som i sin tur kan leda till störningar i vitala system, såsom till exempel kylning av kärnkraftsanläggningar. Den höga säkerhetsnivå som eftersträvas ger upphov till ett behov av tillförlitliga seismiska analyser, även för strukturer som byggs i regioner som traditionellt inte har ansetts som seismiskt aktiva. Fokus i denna licentiatuppsats ligger på områden med seismiska och geologiska villkor som motsvarar de i Sverige och norra Europa. Jordbävningar i Sverige klassas som händelser inom en tektonisk platta som för regioner med hårt berg kan resultera i jordbävningar som domineras av högfrekventa markvibrationer. Sådana högfrekventa vågor propagerar genom bergmassa och jordmaterial och kan där påverka underjordiska strukturer såsom rörledningar.

Syftet med detta projekt är att undersöka vilka parametrar som har stor påverkan på nedgrävda rörledningar som utsätts för högfrekventa seismiska vibrationer. Tyngdpunkten i studien är på rörledningar av armerad betong men stålledningar studeras också i jämförande syfte. Två-dimensionella finita elementmodeller används, utvecklade för dynamisk analys av rörledningar belastas av seismiska vågor som propagerar från berggrunden genom jorden. Modellerna beskriver båda längsgående och tvärgående snitt av rörledningar. Samspelet mellan rörledningar och omgivande jord beskrivs av en icke-linjär modell. De studerade rörledningarna antas vara omgivna av friktionsjord med stor, medel eller liten styvhet. Effekterna av vattenmassa i rören, grundläggningsdjup, jordlagrens tjocklek och varierande jordtjocklek på grund av lutande berggrund studeras. Det visas hur två-dimensionella modellerbaserade på plan töjning kan användas för seismisk analys av rörledningar med cirkulära tvärsnitt.

Resultaten jämförs med de som erhållits för lågfrekventa jordbävningar och förhållandet mellan markrörelseparametrar och responsen hos rörledningar undersöks. Det visas att den naturliga frekvensen för modellerna beror av jordtyp, tjocklek och variation hos jordlagret. Det visas att, särskilt för högfrekventa jordbävningar, olikformigt varierande markdjup på grund av lutande berggrund avsevärt ökar spänningarna i rörledningarna. För de förhållanden som studerats är det klart att det är mindre sannolikt att högfrekvent seismisk belastning ska orsaka skador på nedgrävda rörledningar av betong. Dock är den viktigaste slutsatsen att seismisk analys ändå motiveras, även för rörledningar i områden där jordbävningar med högt frekvensinnehåll förekommer eftersom lokala variationer i markförhållanden kan ha en betydande inverkan på säkerheten.

Nyckelord: Jordbävning, Högfrekvent, Underjordisk, Rörledningar (pipelines), Armerad betong, Lutande berggrund.

Nomenclature

Acronyms

ALA	American Lifeline Alliance
Ch	Chi-Chi
CP	Continuous pipeline
Ds	Dense soil
Du	Duzce
Eu	Eurocode8
PGA	Peak ground acceleration
PGD	Peak ground displacement
PGV	Peak ground velocity
P-waves	Primary wave
RMS	Root-mean-square
R-waves	Rayleigh wave
Se	Sweden
SP	Segmented pipelines
SI	Spectrum intensity
S-waves	Shear waves
Ls	Loose soil
Ms	Medium soil
MMI	Modified Mercalli intensity
NP	Northridge- Pacoima dam station
NR	Northridge- Rancho station

Greek letters

θ	Angle of incidence of the wave with respect to the buried pipeline axis in horizontal plane parallel to the ground surface
α	Adhesion factor
β	The angle of incidence of S-waves
δ'	The interface angle of friction between pipe and soil
γ	Total unit weight of soil
$\bar{\gamma}$	The effective unit weight of soil
λ	Lame's constant
λ_0	The average intensity
υ	Poisson's ratio
ω	Circular frequency
ϕ	The internal friction angle of the soil
ρ	Mass density

$\varepsilon_{\max}$	Maximum axial strain
ξ	Structural damping ratio

Latin letters

A	Total area of all elements around the node considered on the boundary
a , b	Dimensionless parameters for the evaluation of viscous boundary
$\tilde{a}$	Acceleration
a_1, b_1, c_1, d_1, e_1, x_1	Parameters for the evaluation of horizontal bearing capacity factor of soil
$a_{p\theta}$	Peak particle acceleration caused by P-waves
$a_{R\theta}$	Peak particle acceleration caused by R-waves
$a_{s\theta}$	Peak particle acceleration caused by S-waves
c	Apparent wave propagation velocity
c_p	Apparent P-wave propagation velocity
c_s	Apparent S-wave propagation velocity
c_R	Apparent R-wave propagation velocity
C_0	The coefficient of cohesion of backfill soil
C_n	Normal coefficient for viscous boundary
C_t	Tangential coefficient for viscous boundary
D	Outside diameter of pipe
E	Young's modulus
f	The friction factor for various types of pipelines
g	Gravity acceleration
G	Shear modulus
h	Particle displacement of the soil
H	The depth of soil above the centre of the pipeline
I_a	Arias intensity
K_0	Coefficient of soil pressure at rest
$k_{\max}$	Maximum curvature
K_n	Normal coefficient for viscous spring boundary
K_t	Tangential coefficient for viscous spring boundary
N_c , N_q , N_γ	Bearing capacity factors
N_{ch}	Horizontal bearing capacity factor for clay
N_{qh}	Horizontal bearing capacity factor for sandy soil
N_{cv}	Vertical uplift factor for clay

N_{qv}	Vertical uplift factor for sand
p_u	The maximum lateral resistance of soil
$q_{u(up)}$	The maximum vertical uplift resistance of soil
$q_{u(down)}$	The maximum vertical bearing resistance of soil
R	Shortest distance between wave source and plane of the boundary
S_v	Pseudo velocity response spectrum
T_d	The duration of a strong motion
t_u	Maximum axial soil resistance
$\tilde{u}$	Displacement
$\tilde{v}$	Velocity
$v_{s\theta}$	Peak particle velocity caused by S-waves
$v_{p\theta}$	Peak particle velocity caused by P-waves
$v_{R\theta}$	Peak particle velocity caused by R-waves
v_p	Compression wave velocity
v_s	Shear wave velocity
x_u	Ultimate relative displacement in axial direction
y_u	Ultimate relative displacement in vertical direction

Preface

During my study under the supervision by Professor Anders Ansell, I have found a great opportunity to learn how to work systematically. I have had a great time working under Anders's supervision. He runs a group with nice atmosphere, and his expert supervision with continuous support encouraged me to work with high energy. I appreciate and thank you Anders a lot with my sincerest and deepest gratitude.

I would like to thank Professor Stefan Larsson my assistant supervisor at Division of Rock and Soil Mechanics and Dr. Richard Malm my assistant supervisor at the Division of Concrete Structure for helpful advice and support.

I gratefully appreciate Dr. Zilan Zhong at Dept. of Structural and Environmental Engineering, the state university of New York at Buffalo, for nice discussion and comments during my short visit in USA.

I especially thank Dr. Lamis Ahmed, Cecilia Rydell and Daniel Eriksson for nice discussions and my other colleagues for their help. I am also very grateful for the valuable comments on the writing by Professor emeritus Jonas Holmgren.

Last but not least, I would like to send my greatest gratitude to all members of my family and family in law, especially my parents and parents in-law. My lovely family, my husband Asghar and my daughter Masoumeh, please accept my warmest and deepest gratitude; I dedicate my thesis to you.

Appended papers

The thesis contains the following research papers:

I. Abbasiverki, R., Ansell, A., Malm, R., Analysis of shallowly buried reinforced concrete pipelines subjected to earthquake loads. Nordic Concrete Research 51:111-130, 2014.

II. Abbasiverki, R., Ansell, A., Analysis of buried reinforced concrete pipelines subjected to seismic waves, Proceeding of the XXll Nordic Concrete Research Symposium, Iceland, 2014.

III. Abbasiverki, R., Ansell, A., Larsson, S., Seismic response of buried concrete pipelines subjected to high-frequency earthquakes, submitted to Geotechnical and Geological Engineering, June 2016.

In paper I the finite element simulation was done by Abbasiverki with contribution from Malm. The analysis was performed by Abbasiverki. The writing and discussion of results was done by Abbasiverki with contribution from Ansell and Malm. In paper II the analysis and writing was done by Abbasiverki. Ansell assisted with comments on the writing. Paper III was written by Abbasiverki and Ansell, with contribution from Larsson. The finite element modelling was done by Abbasiverki, who evaluated the results in cooperation with Ansell and Larsson.

Table of contents

CHAPTER 6: Numerical Results

CHAPTER 7: Conclusions

CHAPTER 1

Introduction

Pipelines are long tubular structures that are used to transport significant amounts of liquids or gases over long distance. Materials transported by pipelines can be categorized into four groups; oil and gas, potable water and waste water, industrial materials (e.g., ammonia) and materials that are transported in small scale such as biofuels. Pipelines are often buried in the ground, for protection against e.g. severe climate, accidents and sabotage. However, this leads to difficulties in monitoring, maintenance and repair which leads to that a high degree of safety often is associated with pipelines that are important parts of the infrastructure.

1.1 Earthquakes and seismic loads

An earthquake is defined as ground shaking from a sudden release of energy in the earth's lithosphere, i.e. the crust plus part of the upper mantle. There are different reasons for earthquakes such as volcanic activities, the sudden collapse of the roof in a mine/cave, reservoir induced impounding and plate tectonics, but the cause of most earthquakes in the world is plate tectonics. Movements of tectonic plates, both in magnitude and direction, accumulate strain inside the plates and at their boundaries. When the strain reaches its limiting value along a weak region or at plate boundaries or at existing faults, a sudden movement or slip will release the energy of the accumulated strain. This generates elastic waves in the rock mass, which propagate through the elastic medium, and finally reach the surface of the earth. The earthquakes that take place within the boundaries of the tectonic plates are called interplate earthquakes, classified as large earthquakes. The intraplate earthquakes which take place away from the plate boundaries may generate new faults [20, 24].

Earthquake ground motion contains a combination of harmonic motions with various frequencies. The initial level and frequency content of the motion are affected by the source conditions [16]. High-frequency seismic waves are generated by a rupture front focusing at the initial stage of earthquake which causes high slip rate pulses [36]. High frequencies

attenuate quickly in soft soil and propagate further in stiff soils or rocky ground. Herein high-frequency ground motions are referred to as motions dominated by frequencies higher than 10 Hz. Propagation of such high-frequency waves through rock mass and soil medium may affect underground structures such as pipelines and tunnels and when they reach the ground surface they may damage brittle structures and installations [39, 62, 78].

In recent years, the nuclear accidents caused by the Tohoku (Japan) earthquake and the subsequent tsunami on March 11, 2011 brought the attention to seismic analysis of structures within nuclear power plants, even in areas with low seismic activities, such as Sweden and Northern Europe. Earthquakes in Sweden are classified as intraplate events which for regions with hard rock, the motions are associated with high frequencies. It is well documented that earthquakes rarely affect constructions in Sweden. However, earthquakes with small magnitude continuously occur and for a longer time period it is not unlikely that an earthquake with large magnitude that causes a significant risk for constructions may occur. An example of such event occurred in 1904 when an earthquake with magnitude of 5.4 struck near the Koster islands. This event motivated investigation of the possibilities of earthquake damage to constructions in Sweden [13].

The epicentres in Sweden are distributed in three broad geographical zones, of which the Telemark-Vänern zone is the most active, also including the 1904 earthquake. Significant seismic activity is seen in the north, due to a number of neotectonic faults, i.e. faults which have moved since the last ice-age. The Bothnia zone which runs along the Swedish east coast and the Lappland zone in northern Sweden are considered as less active zones. Herein examples of seismic research conducted for structures in Sweden are briefly summarized. For dams in Sweden seismic analysis has not been conducted [40], but seismic hazard assessment has been performed for rockfill and earth dams to discover the possibility of damages. Seismic hazard results show that there is no major risk for dams constructed in south-western Sweden. For high dams built in the middle and northern Sweden, the seismic hazard is small and more investigation is needed for the dams constructed on soil [11]. Most nuclear power plants in Sweden are constructed on hard rock. Ground motions for hard rock areas are dominated by high frequencies, above 10 Hz. Recently, the effect of such high-frequency ground motions on structures and components within nuclear facilities has been studied. The results highlight that the seismic high-frequency earthquakes may be considered as non-damaging for the structures, but may not be insignificant for non-structural components attached to the primary structure [78, 85]. In another project [86], a comparative study has been made between the Eurocode 8 [29] and the Swedish standard [85] for nuclear power plants design. The results indicate that the combination of the Swedish design spectrum with the load combination from the Eurocode 8 gives a more conservative design than the Swedish standard. As a continuation of the described research, the current project focus on dynamic analysis of buried pipelines, which for example can be used for supply of cooling water in nuclear power plants. The pipelines studied are assumed

to be subjected to high-frequency motions, under conditions representative for Sweden and Northern Europe.

Before the 1995 Kobe earthquake, underground structures were considered to be relatively safe during earthquakes but the damage of the Daikai subway station made new concerns at vulnerability of underground structures due to earthquake [14, 22]. During an earthquake buried pipelines may be damaged by deformations caused by wave propagation and or by permanent ground deformation. The latter are in the forms of surface faulting, land sliding, seismic settlement and lateral spreading due to soil liquefaction. An active fault is defined as a discontinuity between two parts of the earth crust. Wave propagation is induced by relative movement along a fault plane. The mass movements of the ground are called landslides that can be caused by seismic shaking. Whenever a loose saturated soil is liquefied by seismic shaking, lateral spreading is created. This liquefaction leads to loss of the shear strength of soil, which results in flowing or lateral movement of liquefied soil. Earthquake induced settlement may be due to densification of dry sand, consolidation of clay or consolidation of liquefied soil. Since the liquefaction-induced ground settlement causes large ground movement, this type of settlement has the largest effect on buried pipelines [67]. Pipeline damage is often due to a combination of wave propagation and permanent ground deformations. For example, in the 1906 San Francisco earthquake half of all observed pipeline damages was due to liquefaction and the other half was from wave propagation. But there have also been some events where pipe damage occurred due to wave propagation only. One example is damage that occurred in Mexico City during the 1985 Michoacan earthquake. The local geology and soil variations in the area caused the damage of large diameter transmission pipelines [27, 67]. Another example is the damage of water pipelines due to the 1999 Chi-Chi (Taiwan) earthquake. In this case 48% of total damage was due to ground shaking, 35% was from faulting, 11% from landslide, and 2% from liquefaction [89].

The work presented in this thesis contributes with a study of the effect from seismic wave propagation on the response of buried pipelines. The finite element method with plain strain element models is used for simulating wave propagation in soil-pipe system with different covering soil types and seismic waves. The focus is on seismic loads dominated by high frequencies and the risk for possible damage to large diameter concrete pipelines.

1.2 Aims and goals

This licentiate thesis aims to identify parameters that significantly affect seismic response of reinforced concrete pipelines due to high-frequency content ground motions dominated by frequencies higher than 10 Hz. Pipe stresses calculated for two different earthquakes, with dominating low and high frequency contents, are compared. Numerical examples are given, with varying soil layer thickness on top of vibrating bedrock, using material

properties representative for Northern Europe and Sweden. The effect from variation in soil stiffness, shape of bedrock, pipeline installation depth and water mass are studied. The response of steel pipelines is also included for comparison. The goal is to demonstrate how a model can be set up for efficient dynamic analysis of buried pipelines subjected to high-frequency seismic loads. The most important research questions are if a two-dimensional FE model can be practically used for accurate analyses, if the effect from the stiffness of the surrounding soil is great and especially if dynamic analyses of these types of pipeline structures subjected to high-frequency seismic loads are important and motivated.

1.3 Contents of the thesis

The thesis consists of seven chapters. Chapter 2 describes structural aspects of pipeline damage. In this chapter typical concrete pipelines and their joints considering manufacturing methods are presented. At the end of the chapter, also manufacturing methods of steel pipelines and typical joints are described. Chapter 3 gives information about strong ground motion parameters such as spectrum intensity and their relationships with pipeline damage. Chapter 4 summarizes methods for seismic analysis of buried pipelines, describing soil-pipe interaction behaviour. In chapter 5, materials, earthquake excitations and finite element models are presented. Chapter 6 gives examples of finite element results. Chapter 7 contains a discussion on the results obtained from the parametric study. General conclusions and further research are presented thereafter. Below the contribution of the appended papers to the thesis is described.

Paper I

Two models of reinforced concrete pipelines which represent longitudinal and transverse cross-sections of pipelines are employed to study the effect of earthquake frequency content and water mass. The analyses are performed for two types of soil with high and medium stiffness.

Paper II

In this paper, a transverse cross-section of a reinforced concrete pipeline is studied. The relationship between spectrum intensity and maximum tensile stress along pipeline cross-section is presented for two different burial depths of pipelines. The example presented is a complement to those given in Paper I.

Paper III

In this paper, the effects of uniform and non-uniform ground are studied. The effect of burial depth and soil layer thickness are investigated. Three levels of soil stiffness are considered for the analysis. All the models are subjected to two different seismic waves.

CHAPTER 2

Buried Pipeline Systems

Piping materials are generally divided into two groups; rigid and flexible. Concrete and steel pipelines are examples of rigid and flexible piping materials, respectively. Compared with steel concrete is an economical and durable material, widely used in water and wastewater networks [63]. In this chapter first damage patterns of pipelines with respect to piping material and joints are described. Typical concrete and steel pipelines which are commonly used in water and waste water networks are described thereafter.

2.1 Structural aspects for pipeline damages

Damage patterns that occur in pipelines are largely dependent on the material base properties and the joint detailing. Accordingly, the pipelines can be divided into two groups; continuous pipelines (brittle) and segmented pipelines (ductile). The continuous pipelines have rigid joints, i.e. the strength and stiffness of the joints are higher than for the pipe barrels. Segmented pipelines have relatively flexible joints. According to empirical data from earthquake loads on pipelines, the damage induced by wave propagation on brittle pipelines is more severe than on ductile pipelines that show 30% of the vulnerability compared with the ductile pipelines [35, 54]. **Table 2.1** and **Figure 2.1** show possible combinations of material and joints and damage pattern that may occur for pipelines.

Table 2.1: Structural aspects on the seismic behaviour of pipelines [54].

Pipelines	Materials	Joints	Damage pattern
Continuous (CP)	Steel; Polyethylene; Polyvinylchloride; Glass Fibre Reinforced Polymer.	Butt welded; Welded Slip; Chemical weld; Mechanical Joints; Special Joints	Tension cracks (Figure 2.3a); Local Buckling (Figure 2.3b); Beam buckling (Figure 2.3c)
Segmented (SP)	Asbestos Cement; Precast Reinforced Concrete/Reinforced Concrete; Polyvinylchloride; Vitrified Clay; Cast Iron; Ductile Iron.	Caulked Joints; Bell end and Spigot Joints; Seismic Joints	Axial Pull-out (Figure 2.3d); Crushing of Bell end and Spigot Joints (Figure 2.3e); Circumferential Flexural Failure and Joint Rotation (Figure 2.3f).

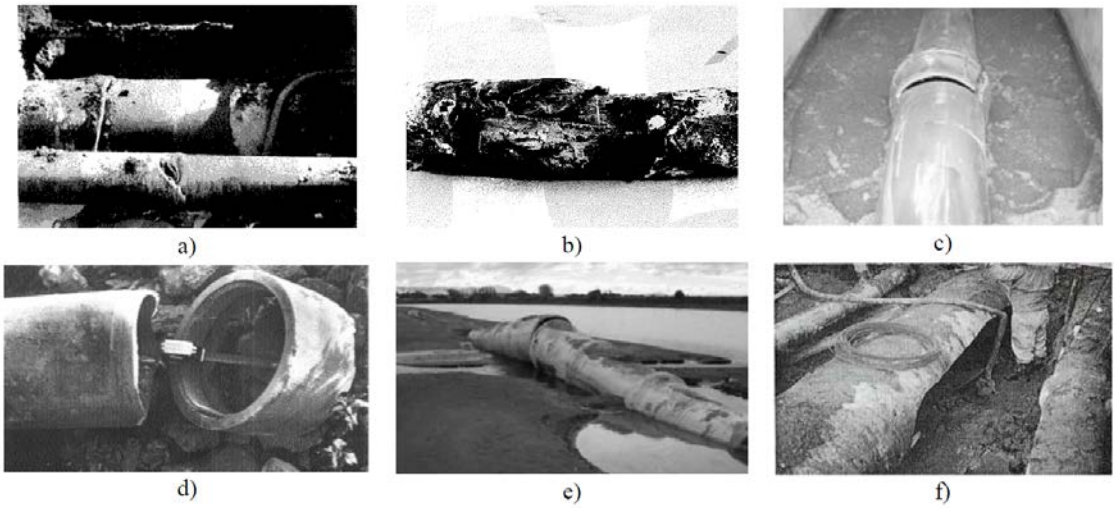

Figure 2.1: Damage patterns for pipelines: a) tension/compression cracks; b) local buckling; c) beam buckling; d) axial pull-out; e) crushing of bell end and spigot joints; f) cracks along the pipe body. From [55].

2.2 Concrete pipelines

Concrete pipelines are designed for pressure flow systems and gravity flow systems. Pressure flow concrete pipe are used to transport and distribute potable water. A sewage system is mostly separated in two parts; sanitary sewers and storm sewers. Gravity-flow concrete pipelines are widely used in sewer systems but some sanitary sewers use pressurized lines since they usually are deeply buried [63].

2.2.1 Gravity-flow concrete pipelines

Reinforced and non-reinforced concrete pipelines are used for gravity systems. The non-reinforced concrete pipelines are typically in sizes ranging from 100 to 1000 mm diameter. Reinforced concrete pipelines consist of one or more cages of steel reinforcement placed in a concrete wall to withstand substantial live and dead loads. Non pressure flow concrete pipelines have concrete joint in bell and spigot shape that are sealed with mastic or rubber gasket. The diameter range for them is almost from 1000 through 4000 mm for pressure range up to 90 kPa. In Sweden, two typical concrete pipelines are used in sanitary and storm sewers system. These are the non-reinforced concrete pipeline KANMAX and the steel reinforced concrete pipeline GERMAX with bell and spigot joint sealed with rubber gasket as shown in **Figure 2.2 [**79].

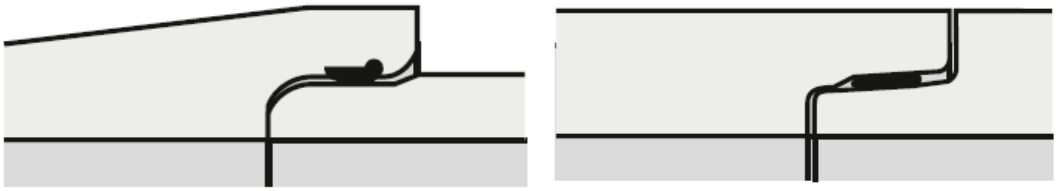

KANMAX GERMAX

Figure 2.2: Typical joints for non-pressurized concrete pipelines. Reproduced from [79].

2.2.2 Pressure-flow concrete pipelines

Concrete pressure pipelines include various types of wall constructions. These are pre-stressed cylinder pipelines, reinforced cylinder pipelines, pre-stressed non-cylinder pipelines, reinforced non-cylinder pipelines, and bar-wrapped cylinder pipelines. The general description of these pipelines is based on whether or not the pipe has a full-length steel cylinder and whether it is conventionally reinforced with deformed bars, wire, or smooth bars, or pre-stressed with high-strength wire. Pre-stressed cylinder/non-cylinder pipelines are typically in sizes ranging from 500 mm to 4000 mm diameter. Reinforced cylinder pipelines are in sizes ranging from 250 mm to 4000 mm. Bar-wrapped cylinder pipelines are in sizes ranging from 250 mm to 1850 mm [4, 31, 32].

In construction of pre-stressed cylinder pipelines, a steel cylinder can be lined with a concrete core or be embedded in a concrete core, see **Figure 2.3**. In both types of construction, manufacturing begins with a full-length welded steel cylinder. Joint rings are attached to each end and then the steel cylinder is hydrostatically tested. A concrete core is placed either by vertical casting for embedded cylinders or through a centrifugal process for

lined cylinders. After the core is cured, the pipe is helically wrapped with high strength, hard-drawn wires and coated with dense cement mortar. Pre-stressed non-cylinder pipelines include a concrete core in which either steel reinforced or longitudinally prestressed wire is embedded and then circumferential prestressing wire is wound around the outside of the core, see **Figure 2.4** [31].

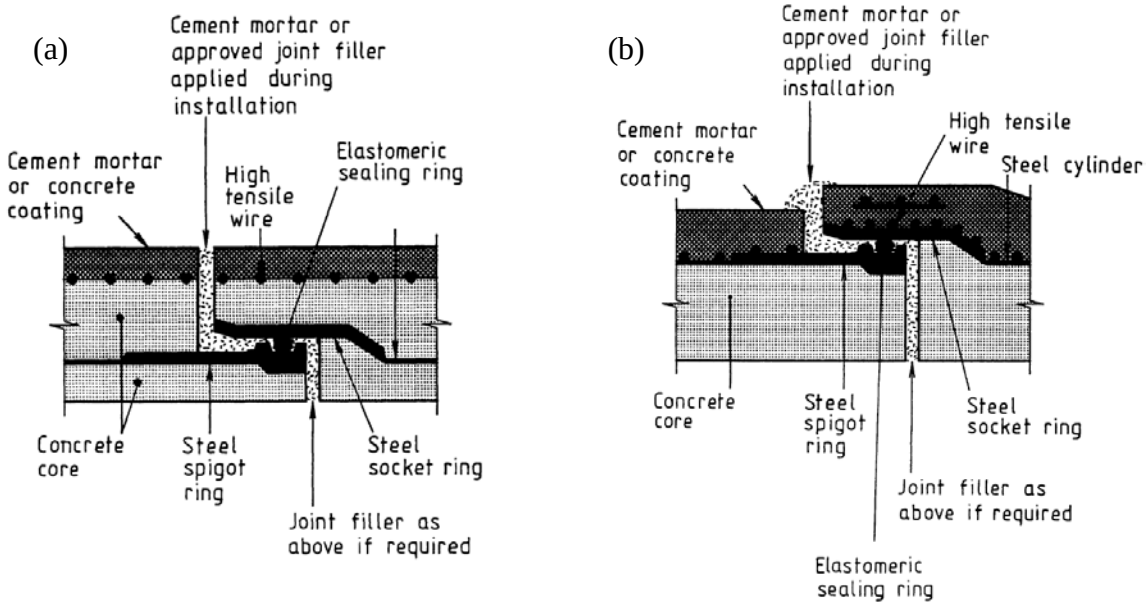

Figure 2.3: Prestressed cylinder pipeline: a) Lined Cylinder Pipeline and b) Embedded Cylinder Pipeline. Reproduced from [31].

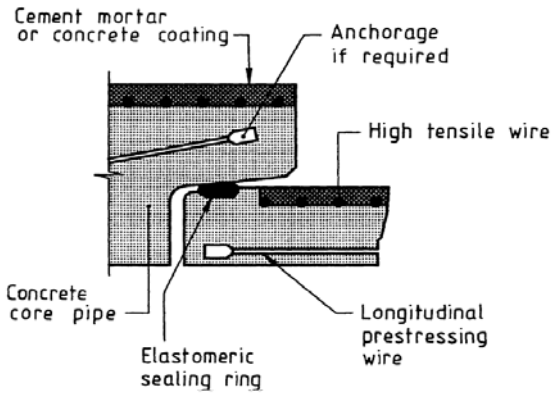

Figure 2.4: Prestressed non-cylinder pipeline. Reproduced from [31].

Reinforced cylinder pipelines consist of a steel cylinder and one or more cages of steel reinforcement embedded in concrete. Reinforced non-cylinder pipelines include one or more cages of steel reinforcement. The joints have bell and spigot shape with steel joint rings sealed with a confined round rubber gasket or formed gasketed concrete joint, see **Figure 2.5.**

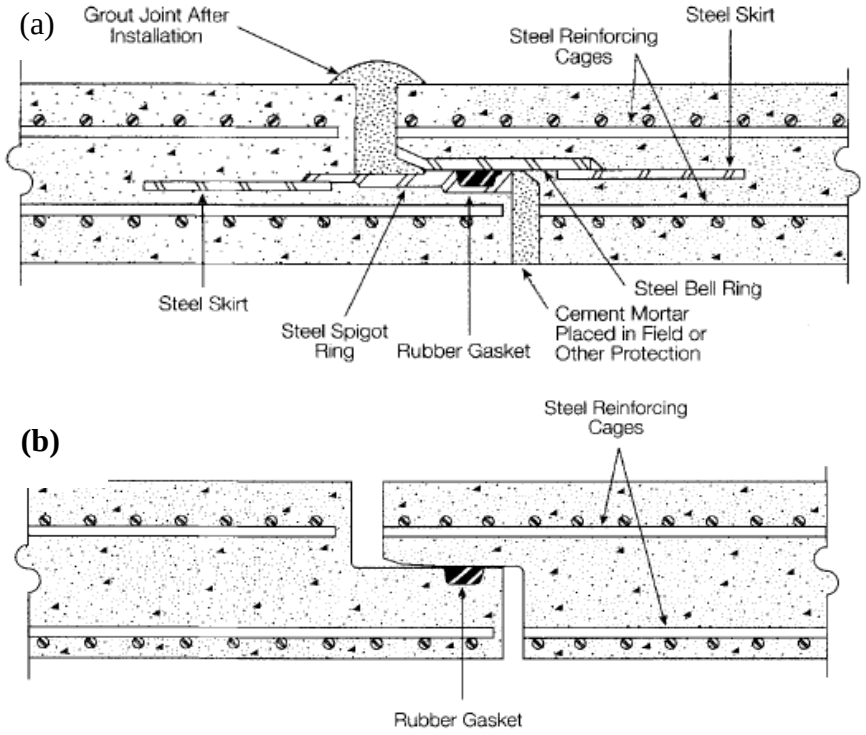

Figure 2.5: Reinforced concrete non-cylinder pipelines: a) Pipe with Steel Joint Rings and b) Pipe with Concrete Joint Rings. Reproduced from [4].

Bar-wrapped cylinder pipelines consist of a steel cylinder lined with concrete or cement mortar, then helically wrapped with a mild steel bar and coated with dense cement mortar. Bar-wrapped cylinder pipelines and lined cylinder types have different structural components to carry the loads. Bar-wrapped cylinder pipelines are essentially a steel pipeline that is stiffened with steel reinforcing bars [8]. An easily assembled watertight joint is provided by using bell and spigot steel joint rings welded to the ends of the cylinder and sealed with a confined round rubber gasket, see **Figure 2.6**.

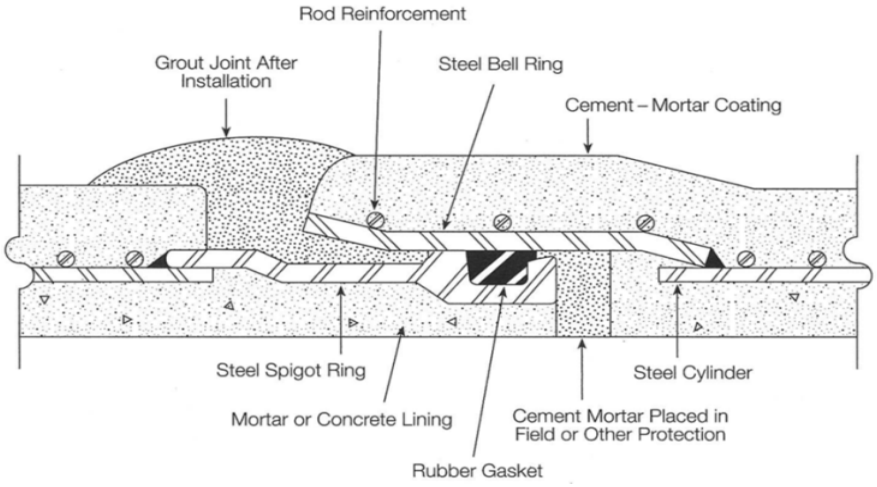

Figure 2.6: Concrete bar-wrapped cylinder pipeline. Reproduced from [4].

2.3 Steel pipelines

Steel pipelines have a variety of applications such as transport of water, wastewater, oil and gas but also for structural piling and supports [46]. The steel pipelines are generally made in two types; welded steel pipelines or seamless steel pipelines. The seamless type is commonly used for high pressure applications such as gas transmission lines [34]. Herein, welded water steel pipelines will be described. Steel water pipelines are typically manufactured in the size range from 100 mm to more than 3660 mm in diameter. There are commonly two methods for manufacturing water steel pipelines, as spiral seam pipelines and straight seam pipelines. Spiral seam pipelines are produced from coiled strips of steel through a continuous process, see **Figure 2.7**.

Straight seam pipelines are manufactured from plates or sheets with parallel edges, see **Figure 2.8** [5, 10, 33]. Common types of joints for steel pipelines are butt welded joints, welded spigot and socket (sleeve) joints (**Figure 2.9 (a)** and **(b)),** welded collars, flange joints **Figure 2.9 (c)**, spigot and socket joints with seal, flexible couplings (e.g. Viking Johnson type) and push fit joints [30,76].

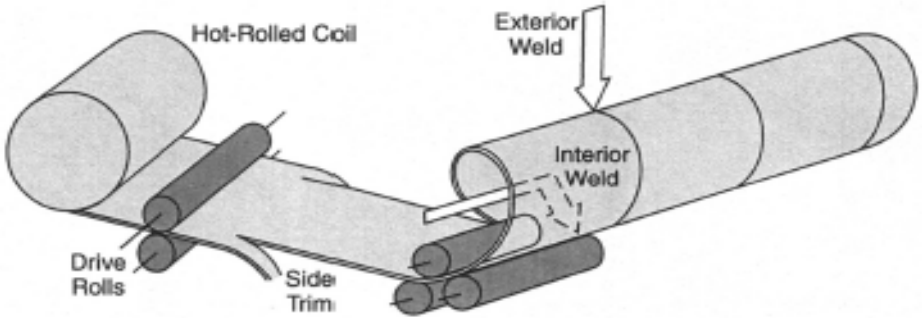

Figure 2.7: Schematic process diagram for making a spiral seam steel pipeline. Reproduced from [5].

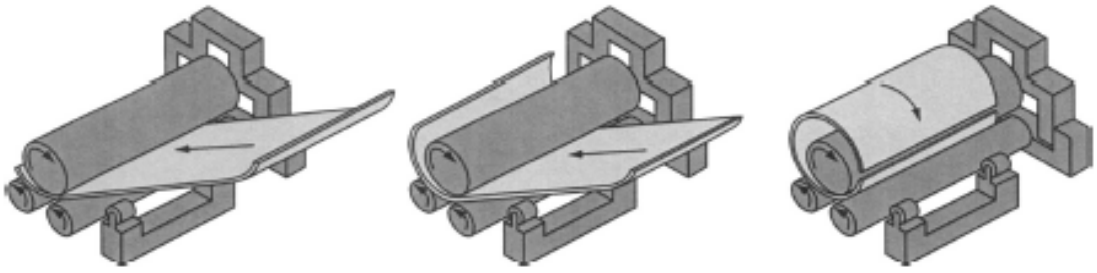

Figure 2.8: Schematic diagram for making a steel plate pipeline. Reproduced from [5].

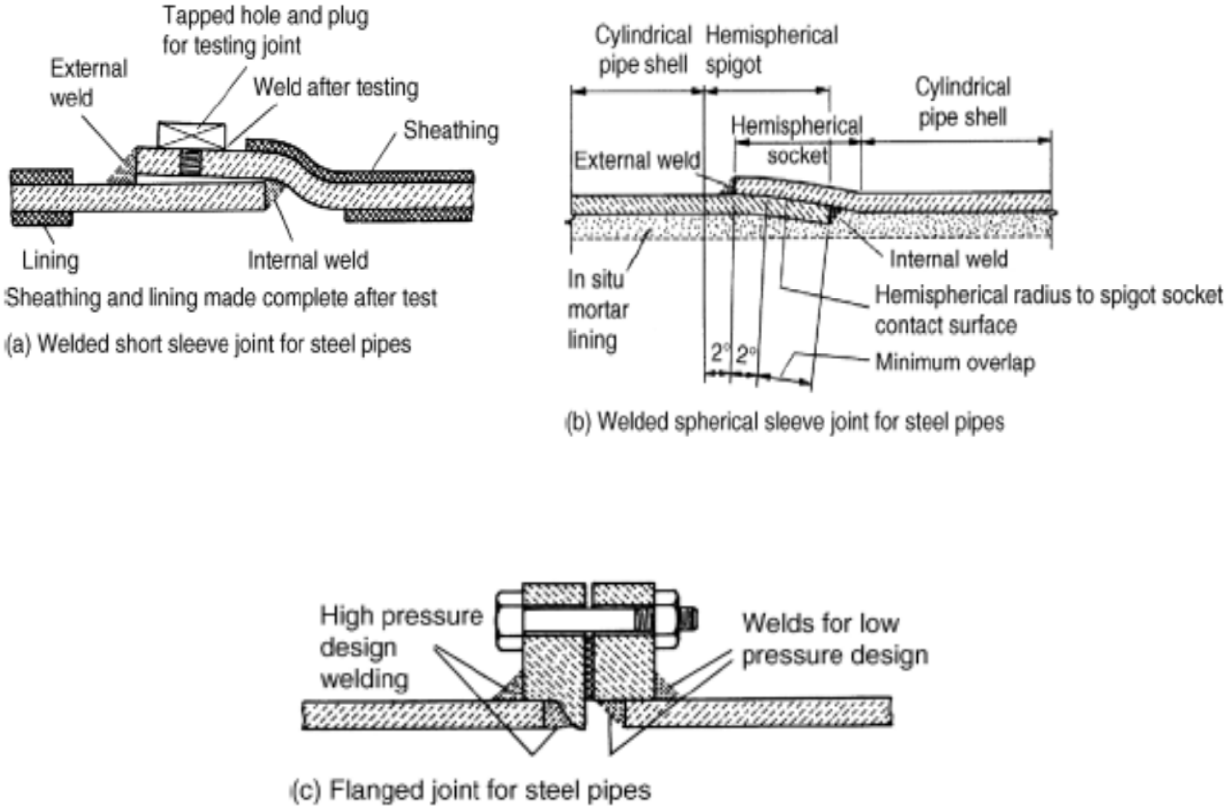

Figure 2.9: Typical steel pipe joints. Reproduced from [76].

CHAPTER 3

Strong Ground Motion Parameters Related to Pipeline Damage

The buried pipeline damage depends on various factors one of which is the intensity of the earthquake. The intensity of earthquake is usually defined by strong ground motion parameters. In this chapter, strong ground motion parameters and their importance for pipeline damage is described.

3.1 Strong ground motion parameters

The ground motions produced by earthquake have three components of translation and three components of rotation. But in practice, they are most commonly described by three orthogonal components of translational motion. Three primary significant characteristics of earthquake ground motions are: amplitude, frequency content and duration of vibrations.

3.1.1 Amplitude parameters

The earthquake ground motion is typically described with a time history, for acceleration, velocity or displacement. Typically one of them is measured directly and the other ones derived by integration and/or differentiation of a measured time history. The acceleration time history often contains a significant portion of relatively high frequencies. Integration has a smoothing and filtering effect, as can be seen in the frequency domain. The velocity and acceleration are calculated as:

$$\tilde{v}(\omega) = \tilde{a}(\omega)/\omega \tag{3.1}$$

$$\tilde{u}(\omega) = \tilde{v}(\omega)/\omega \tag{3.2}$$

Where $\tilde{u}$, $\tilde{v}$ and $\tilde{a}$ are displacement, velocity and acceleration, respectively. The velocity-time history thus shows less high-frequency content compared to the acceleration-time history. The displacement time history is dominated by relatively low frequencies as it is obtained by another round of integration. **Figure 3.1** illustrates examples of acceleration, velocity and displacement time histories of earthquake ground motions.

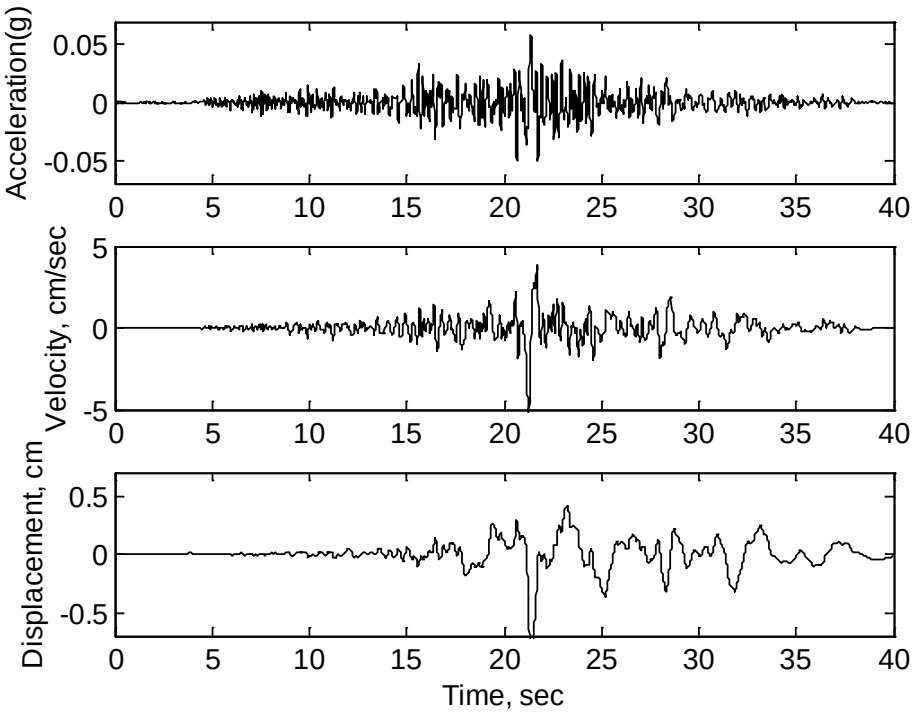

Figure 3.1: Acceleration, velocity and displacement time histories for the CUC-180 components of the Northridge earthquake [Paper I].

Peak ground acceleration (PGA), peak ground velocity (PGV) and peak ground displacement (PGD) are the most common amplitude parameters. Acceleration is directly related to inertial forces and therefore the largest dynamic forces induced in very stiff structures are related to PGA. PGV is dominated by the intermediate frequency range and is more suitable for structures or facilities such as tall or flexible building and bridges. Since it is difficult to determine PGD accurately, due to signal processing errors for filtering and integration of acceleration time histories and due to long period noise, it is less commonly used as a strong ground motion parameter [52].

3.1.2 Frequency content parameters

The earthquake ground motion contains a broad range of frequencies. Fourier spectra, power spectra and response spectra are used to characterize the earthquake ground motion in frequency domain. The Fourier amplitude spectrum and power spectrum density completely describe a ground motion. The response spectrum does not present the ground motion, but it describes potential effects of a ground motion on structures. An example of spectral parameters is predominating period. The period of ground motion corresponding to the maximum value of the Fourier amplitude spectrum is called predominate period. While the predominate period gives some information about frequency content but cannot completely describe frequency contents of ground motion, two different frequency contents motions can have the same frequency content, see **Figure 3.2**.

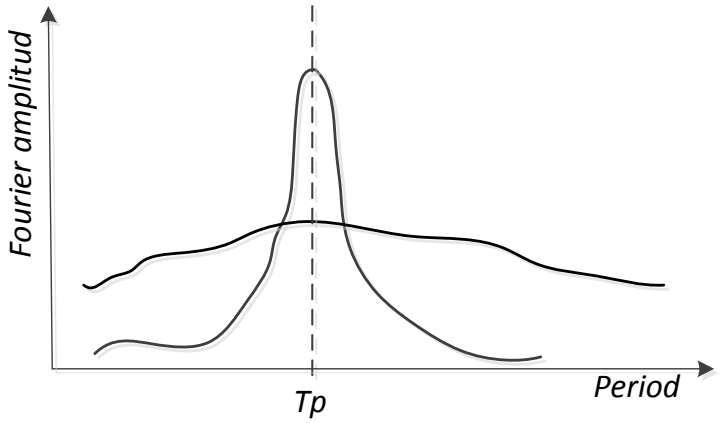

Figure 3.2: Two hypothetical Fourier amplitude spectra with the same predominated period but very different frequency contents [52].

$\mathrm{PGV}/\mathrm{PGA}$ is another parameter that explains the frequency content of ground motion. The period of vibration for a simple harmonic motion can be obtained from $2\pi\left(\mathrm{PGV}/\mathrm{PGA}\right)$. For earthquake ground motions, this value indicates the most significant period.

3.1.3 Duration

The duration of an earthquake depends on the time which is needed to release the accumulated strain energy by a movement across the fault. The duration of strong ground motions may significantly affect the damage generated by earthquake. The number of loading or stress reversals which occur during an earthquake is a key importance because many physical processes (e.g. the degradation of stiffness and strength of structures) are

sensitive to them. Therefore, the motions having long duration and moderate amplitude can produce enough load reversals to cause substantial damage. In contrast, the motions with short duration may not produce enough load reversals to cause damage, even if the amplitude of motion is high enough.

3.1.4 Other ground motion parameters

The ground motion parameters explained in the previous sections describe the amplitude, frequency content or duration of an earthquake ground motion. Due to the importance of all these parameters, parameters that are related to more than one are very useful. Root-mean-square (RMS) acceleration [60], Arias intensity [7] and spectrum intensity [45] are examples that describe amplitude and frequency content of earthquake.

The RMS acceleration includes the effect of amplitude and frequency content of earthquakes, defined as

$$a_{RMS} = \sqrt{\frac{1}{T_d}\int_0^{T_d}\left[a(t)\right]^2 dt} = \sqrt{\lambda_0} \tag{3.3}$$

where g is the gravity acceleration, T_d the duration of a strong motion and λ_0 the average intensity (or mean squared acceleration). The RMS parameter is sensitive to the method used for defining ground motion duration.

The Arias intensity is closely related to the RMS acceleration but it is calculated by integration over the entire duration. Therefore, its value is independent from the duration of strong motion. The Arias intensity is in velocity units and defined as

$$I_a = \frac{\pi}{2g}\int_0^{\infty}\left[a(t)\right]^2 dt \tag{3.4}$$

Spectrum intensity is the area under the pseudo velocity response spectrum (S_v) within the period range 0.1-2.5 sec as many structures have fundamental periods in this range. Spectrum intensity can be computed for any structural damping ratio (ξ). This parameter is in displacement dimension and if divided by 2.4 sec it gives a value in a velocity dimension, i.e. as:

$$SI = \frac{1}{2.4}\int_{0.1}^{2.5} S_v(T,\xi)\,dT \tag{3.5}$$

3.2 Pipeline damage indicators

The damage of buried pipelines depends on earthquake intensity. Various types of seismic parameters are employed to present pipeline damage. The most common parameters are modified Mercalli intensity (MMI), peak ground acceleration (PGA) and peak ground velocity (PGV). Peak ground velocity has a closer relationship with pipeline damage than modified Mercalli intensity and peak ground acceleration; this is due to its relationship with ground strain, the main cause of pipeline damage during wave propagation. Modified Mercalli intensity was used for describing pipeline damages in the 80s and 90s before the installation of seismic stations and the availability of seismic records. Peak ground acceleration is related to inertial forces generated by motion of buried pipelines which are much smaller than the forces induced by the soil deformation, see [29, 53]. PGA has been used for analysing pipeline damage for cases when PGV attenuation laws are limited [26, 49, 73, 74, 75]. The other parameters that have been used as damage indicator are for example PGV^2/PGA and spectrum intensity. The PGV^2/PGA parameter is in displacement dimension which is related to very low frequency contents. This parameter was proposed e.g. to demonstrate the damage in the 1985 Michoacan event for soft soils, since PGV^2/PGA had better correlation to pipeline damage than PGV for soft soils [72]. In Japan, to avoid secondary disasters caused by gas leaks, a device called spectrum intensity sensor for gas supply networks has been designed. When monitored SI values exceed 30 to 40 cm/sec, the gas supply is stopped automatically [65].

CHAPTER 4

Seismic Analysis of Buried Pipelines

Propagation of seismic waves in soil causes two types of deformations [70]; 1) Axial deformation caused by the components that propagate along the pipeline axis and, 2) Bending deformation generated by the components of the waves that propagate in a direction perpendicular to the longitudinal axis. Different methods have been proposed for buried pipeline analysis from simple ones neglecting soil-pipe interaction to complicated Finite Element (FE) Models.

4.1 Seismic analyses of buried pipelines by neglecting soil-pipe interaction

Newmark [61] presented a simplified method for calculating the pipe deformations due to wave propagation. In this method, it is assumed that the pipe follows the soil deformation without slippage and interaction. Therefore, it gives the upper bound estimate of the strains in the pipeline. When a wave propagates with the wave velocity c relative to the ground surface (apparent wave propagation velocity), along the longitudinal axis (x-axis) of the buried pipeline, the particle displacement of the soil (h) is a function of $(x - ct)$:

$$h = f(x - ct) \tag{4.1}$$

The various derivatives of the displacement h with respect to x and t are given by the following relations:

$$\frac{\partial h}{\partial x} = f'(x - ct) \tag{4.2}$$

$$\frac{\partial^2 h}{\partial x^2} = f''(x - ct) \tag{4.3}$$

$$\frac{\partial h}{\partial t} = -cf'(x - ct) \tag{4.4}$$

$$\frac{\partial^2 h}{\partial t^2} = c^2 f''(x - ct) \tag{4.5}$$

From Eqs. (4.2) and (4.4) the following results can be derived:

$$\frac{\partial h}{\partial x} = -\frac{1}{c}\frac{\partial h}{\partial t} \tag{4.6}$$

$$\frac{\partial^2 h}{\partial x^2} = \frac{1}{c^2}\frac{\partial^2 h}{\partial t^2} \tag{4.7}$$

In the case where h is in the direction of *x*, the axial strain is obtained from equation Eq. (4.6) and the maximum axial strain is therefore:

$$\varepsilon_{\max} = -\frac{PGV}{c} \tag{4.8}$$

In the case where h is perpendicular to the pipe axis (*x*), both horizontally or vertically, maximum curvature is obtained from equation Eq. (4.7) and it follows that:

$$k_{\max} = \frac{PGA}{c^2} \tag{4.9}$$

Equations (4.8) and (4.9) are widely used for seismic design of buried pipelines [3, 29, 48]. When there is an angle in the horizontal plane between the pipe axis and the direction of propagation, the axial strain and curvature are calculated from **Table 4.1**, where $v_{p\theta}$ and $a_{p\theta}$ are peak particle velocity and peak particle acceleration caused by P-waves, c_p is the apparent P-wave propagation velocity, $v_{s\theta}$ and $a_{s\theta}$ are the peak particle velocity and peak particle acceleration caused by S-waves, c_s is the apparent S-wave propagation velocity, $v_{R\theta}$ and $a_{R\theta}$ are the peak particle velocity and peak particle acceleration caused by R-waves, c_R is the apparent R-wave propagation velocity and θ is the angle of incidence of the wave with respect to the buried pipeline axis in horizontal plane parallel to the ground surface [94].

Table 4.1: Summary of strain induced in pipelines, neglecting the soil-pipe interaction [94].

Wave type		Longitudinal strain	curvature
P-wave		$\varepsilon = \pm\left(v_{p\theta}/c_p\right)\cos^2\theta$ $\varepsilon_{\max} = \pm\left(v_{p\theta}/c_p\right)$ for $\theta = 0$	$k = \pm\left(a_{p\theta}/c_p{}^2\right)\sin\theta\cos^2\theta$ $k_{\max} = \pm\left(a_{p\theta}/c_p{}^2\right)$ for $\theta = 35^\circ 16'$
S-wave		$\varepsilon = \pm\left(v_{s\theta}/c_s\right)\sin\theta\cos\theta$ $\varepsilon_{\max} = \pm\left(v_{s\theta}/c_s\right)$ for $\theta = 45^\circ$	$k = \pm\left(a_{s\theta}/c_s{}^2\right)\cos^3\theta$ $k_{\max} = \pm\left(a_{s\theta}/c_s{}^2\right)$ for $\theta = 0$
Rayleigh wave	Compressional component	$\varepsilon = \pm\left(v_{R\theta}/c_R\right)\cos^2\theta$ $\varepsilon_{\max} = \pm\left(v_{R\theta}/c_R\right)$ for $\theta = 0$	$k = \pm\left(a_{R\theta}/c_R{}^2\right)\sin\theta\cos^2\theta$ $k_{\max} = \pm\left(a_{R\theta}/c_R{}^2\right)$ for $\theta = 35^\circ 16'$
	Shear component		$k = \pm\left(a_{R\theta}/c_R{}^2\right)\cos^2\theta$ $k_{\max} = \pm\left(a_{R\theta}/c_R{}^2\right)$ for $\theta = 0$

4.2 The apparent wave propagation velocity

The ground motion propagating under the soil surface includes a mixture of body (compression, shear) and surface (Rayleigh, Love, etc) waves. Shear waves (S-waves) and Rayleigh waves (R-waves) are considered for seismic analysis of buried pipelines since for body waves, shear waves carry more energy and generate larger ground motion than compression waves and for surface waves, axial strain induced by Rayleigh waves in the pipeline is significantly higher than that of the bending strain induced by Love waves. The type of seismic waves for seismic design of pipelines is selected based on the focal depth and the distance between the focus and the site, i.e. epicentre distance. The velocity of Rayleigh wave (R-wave) is considered for the sites with epicentre distance more than five times focal depth. Otherwise, the velocity of shear waves (S-wave) is used for seismic analysis, see **Figure 4.1** [48, 69].

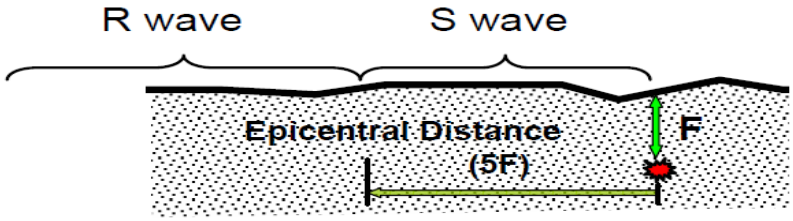

Figure 4.1: Considerations for S-wave and R-wave in pipeline design [48].

When the body waves are incident from the half-space to the bottom layer of the site, with seismic waves traveling through the softer layers, the refraction causes a concave travel path. By the time they reach the surface, the angle of incidence is usually very small with respect to the vertical (**Figure 4.2**).

The apparent wave propagation velocity of shear waves is thus many times higher than the shear wave velocity for the surface materials. If the angle of incidence of S-waves is β for the shear wave velocity for the surface materials equal to C_s, the apparent wave propagation velocity ($C_{s\_apparent}$) for shear waves can be calculated as:

$$C_{s\_apparent} = \frac{C_s}{\sin\beta} \tag{4.10}$$

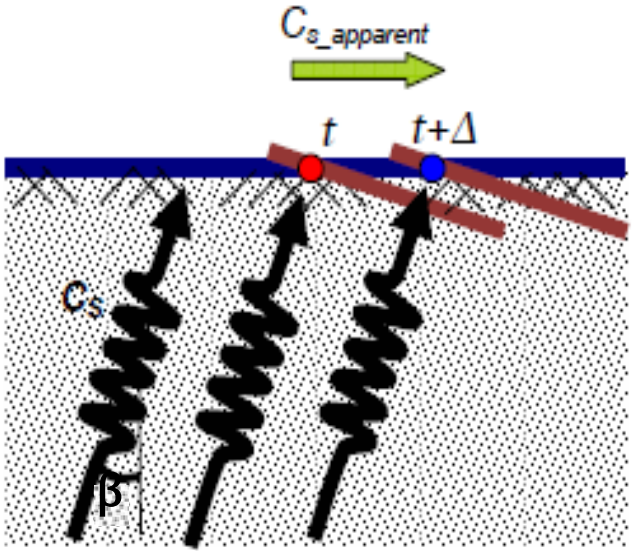

Figure 4.2: The apparent seismic wave propagation of S-wave [48].

For the Rayleigh waves, the apparent wave propagation velocity ($C_{r\_apparent}$) is equal to the phase velocity of Rayleigh waves (C_{r_ph}) due to the traveling path of the Rayleigh waves which is always parallel to the ground surface (**Figure 4.3**).

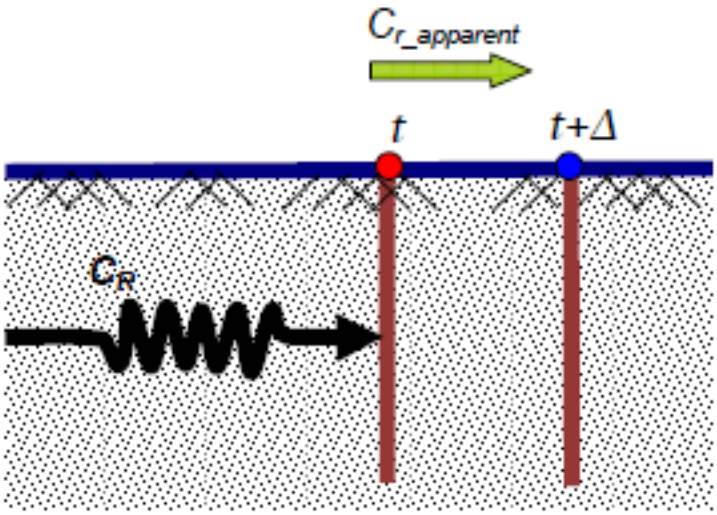

Figure 4.3: The apparent seismic wave propagation of R-wave [48].

4.3 Analytical models, accounting for soil-pipe interaction

Different models have previously been employed for seismic analysis of buried pipelines considering soil-pipe interaction:

1) Quasi-static analysis with soil-structure interaction in which a soil-pipeline interaction system is modelled as a beam embedded in an infinite isotropic homogeneous elastic-plastic medium or surrounded by soil springs by neglecting inertial and damping terms in the dynamic equation [90, 91].

2) Dynamic analysis by considering the theory of beams on elastic foundations. In this method, the pipe is modelled with a lumped mass model and soil-pipe interaction is considered with a spring dashpot system whose reactions derived from static and dynamic continuum theories [18, 19, 41, 42, 66].

3) Dynamic analysis by considering shell theory with soil-structure interaction [21, 50, 51, 64, 88, 94].

4) Three-dimensional finite element analysis where the pipe is modelled with shell elements and soil-pipe interaction is considered by the modelling soil around pipe [93].

5) Beam on Nonlinear Winkler Foundation (BNWF) model, where the pipe is modelled with beam or shell elements and the soil is represented by independent springs, lumped at discrete locations of the pipe. This method was proposed by the American Lifelines Alliance (ALA) and recently many authors have implemented it [43, 44, 56, 77, 80, 81, 82].

Model 1 and 2 cannot evaluate the distribution of stress around the pipeline cross-section. From model 3 and 4, the possibility of considering cross-section deformation exists. However, the solution procedures contain a series of equations, which in turn require intensive computational effort. From Model 5, the pipeline cross-section distortion can be obtained but it has some limitations, such as for modelling the lateral variation of local soil. To cover this, in this project two-dimensional plain strain models are implemented where the interaction at the soil and pipe interface are modelled using springs with behaviour as proposed by the ALA guideline. Through this model, both longitudinal and transverse cross-sections of pipelines are modelled considering the lateral variation of local soil.

4.4 Soil-pipe interaction model

The soil-pipe interaction model proposed by the American Lifeline Alliance (ALA) consists of springs that are distributed in three perpendicular directions with respect to the pipe, see **Figure 4.4**. The springs have elastic-plastic behaviour which can describe the slip of pipelines in the soil when the earthquake is strong [3].

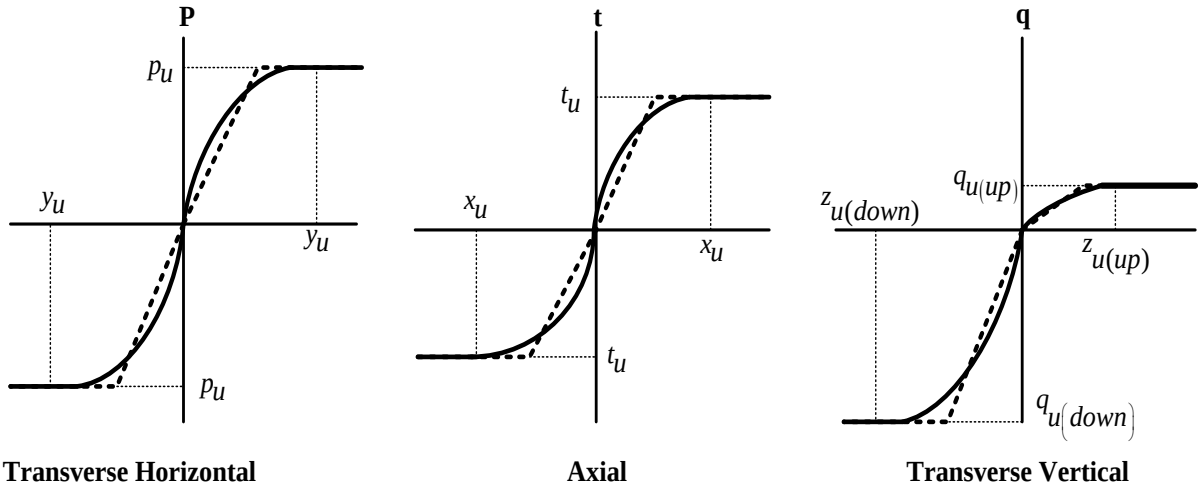

Figure 4.4: Load-deformation relationships for spring elements representing soil-pipeline interaction.

Axial spring

Maximum soil resistance to movement in the pipe axial direction is given in units of force per unit length of pipe, as:

$$t_u = \pi D c_o \alpha + \pi D H \bar{\gamma} \frac{1+K_0}{2} \tan\delta' \tag{4.11}$$

$$\alpha = 0.608 - 0.123 c_o - \frac{0.274}{c_o^{\,2}+1} + \frac{0.695}{c_o^{\,3}+1} \tag{4.12}$$

These soil springs are picked up from pile shaft load transfer theory, where D is the outside diameter of pipe, c_o the coefficient of cohesion of backfill soil, H the depth of soil above the centre of the pipeline, $\bar{\gamma}$ is the effective unit weight of soil, α an adhesion factor, $\delta' = f \times \phi$ the interface angle of friction between pipe and soil, ϕ the internal friction angle of the soil, f the friction factor for various types of pipelines (**Table 4.2**) and $K_0 = 1 - \sin\phi$ is a coefficient of soil pressure at rest. An ultimate relative displacement (x_u) corresponding to maximum soil resistance (t_u) is 3 to 5 mm for sand and 8 to 10 mm for clays.

Table 4.2: Friction factor f for various external coatings [3].

Pipe Coating	f
Concrete	1.0
Coal Tar	0.9
Rough Steel	0.8
Smooth Steel	0.7
Fusion Bonded Epoxy	0.6
Polyethylene	0.6

Lateral Soil Spring

The maximum lateral resistance of soil per unit length of pipe can be calculated as:

$$p_u = N_{ch} c_o D + N_{qh} \bar{\gamma} H D \tag{4.13}$$

$$N_{ch} = a_1 + b_1 x_1 + \frac{c_1}{(x_1+1)^2} + \frac{d_1}{(x_1+1)^3} \le 9 \tag{4.14}$$

$$N_{qh} = a_1 + b_1 x_1 + c_1 x_1^{\,2} + d_1 x_1^{\,3} + e_1 x_1^{\,4} \tag{4.15}$$

These soil springs are picked up from footing and vertical anchor plate pull-out capacity theory and laboratory tests on model pipelines simulating horizontal pipe movements. Here, N_{ch} is a horizontal bearing capacity factor for clay (zero for c_o = 0) and N_{qh} a horizontal

bearing capacity factor for sandy soil (zero for ϕ=0). Relative displacement y_u at p_u, can be determined by:

$$y_u = 0.04\left(H + \frac{D}{2}\right) \leq 0.01D \quad \text{to} \quad 0.02D \tag{4.16}$$

The above parameters are found in ALA [3] and are here listed in **Table 4.3**.

Table 4.3: Parameters for the evaluation of N_{ch} and N_{qh} from [3]

Factor	ϕ	x_1	a_1	b_1	c_1	d_1	e_1
N_{ch}	0	H/D	6.752	0.065	-11.063	7.119	-
N_{qh}	20	H/D	2.399	0.439	-0.03	$1.059\cdot10^{-3}$	$-1.754\cdot10^{-3}$
N_{qh}	25	H/D	3.332	0.839	-0.090	$5.606\cdot10^{-3}$	$-1.319\cdot10^{-3}$
N_{qh}	30	H/D	4.565	1.234	-0.089	$4.275\cdot10^{-3}$	$-9.159\cdot10^{-3}$
N_{qh}	35	H/D	6.816	2.019	-0.146	$7.651\cdot10^{-3}$	$-1.683\cdot10^{-3}$
N_{qh}	40	H/D	10.959	1.783	0.045	$-5.425\cdot10^{-3}$	$-1.153\cdot10^{-3}$
N_{qh}	45	H/D	17.658	3.309	0.048	$-6.443\cdot10^{-3}$	$-1.299\cdot10^{-3}$

Vertical Soil Spring

The soil spring properties are different for uplift and bearing cases. The maximum soil resistance per unit length of the pipeline in vertical uplift can be calculated as:

$$q_{u(up)} = N_{cv} c_o D + N_{qv} \overline{\gamma} HD \tag{4.17}$$

$$N_{cv} = 2\left(\frac{H}{D}\right) \leq 10 \quad \text{for} \quad \left(\frac{H}{D}\right) \leq 10 \tag{4.18}$$

$$N_{qv} = \left(\frac{\phi H}{44D}\right) \leq N_q \tag{4.19}$$

The properties of these soil springs are from pull-out capacity theory and laboratory tests on anchor plates and models of buried pipelines, where N_{cv} is a vertical uplift factor for clay (0 for $c_o = 0$) and N_{qv} is a vertical uplift factor for sand (0 for ϕ = 0º). The mobilizing displacement of soil, $z_{u(up)}$ at $q_{u(up)}$ can be taken as $0.01H$ to $0.02H$ for sands and $0.1H$ to $0.2H$ for clay. The maximum soil resistance per unit length of pipeline in vertical bearing can be calculated as:

$$q_{u(down)} = N_c cD + N_q \overline{\gamma} HD + N_\gamma \gamma \frac{D^2}{2} \tag{4.20}$$

$$N_c = \left(\cot\left(\phi + 0.001\right)\right)\left(\exp\left[\pi \tan\left(\phi + 0.001\right)\right]\tan^2\left(45 + \frac{\phi + 0.001}{2}\right) - 1\right) \tag{4.21}$$

$$N_q = \exp\left[\pi \tan\phi\right]\tan^2\left(45 + \frac{\phi}{2}\right) \tag{4.22}$$

$$N_\gamma = \exp\left[0.18\phi - 2.5\right] \tag{4.23}$$

These soil springs are picked up from bearing capacity theory for footings, where N_c, N_q and N_γ are bearing capacity factors and γ is the total unit weight of soil. The soil displacement, $z_{u(down)}$ at $q_{u(down)}$ can be taken as $0.1D$ for granular soils and $0.2D$ for cohesive soils.

CHAPTER 5

Dynamic Finite Element Analysis

In this chapter, two-dimensional (plain strain) dynamic FE models of pipeline-soil system employed in papers I-III are presented, where material properties, seismic excitation, boundary condition, damping of the system and FE modelling are described.

5.1 Material properties

In this project, a reinforced concrete pipeline GERMAX [79], with 1200 mm nominal diameter and 135 mm wall thickness (t) has been used for the analyses. Material qualities C45/55 and B500B are assigned for the concrete and steel reinforcement, respectively. It is assumed that the joints have strengths equal to the pipeline barrel so that the entire concrete pipeline shows continuous properties. A steel pipeline with arc welded joints is compared with reinforced concrete pipeline [77]. The steel pipeline has 1067 mm diameter and 12.7 mm thickness. The material type X-60 is assumed for the steel. Three types of frictional soil with properties similar to Swedish are adopted for simulating soil around pipelines; first one with low stiffness, second one with medium stiffness and third one with high stiffness. For the properties of granite rock for the case with inclined bedrock, see **Table 5.1** [2, 38].

Table 5.1: Soil and rock properties.

Soil-Rock type	Density (kg/m^3)	Average shear wave velocity (m/s)	Friction angle	Young's modulus (GPa)
Loose (Ls)	1400	75	28°	0.021
Medium(Ms)	1800	250	38°	0.293
Dense (Ds)	2200	450	45°	1.158
Granite	2500	2600	-	40

5.2 Seismic excitation

The seismic excitation in this study is represented by acceleration-time histories. Seven input ground motions have been employed in this study, see **Table 5.2**.

Table 5.2: Ground motion parameters [84].

Location	PGA (g)	PGV (cm/sec)	PGD (cm)	Predominate period (sec)	Velocity spectrum intensity($\xi = 5\%$) (cm/sec)
Sweden (Se)	0.146	2.99	0.61	0.08	3.72
Eurocode8 (Eu)	0.290	19.01	4.43	0.30	38.98
Duzce (Du)	0.052	4.79	4.82	0.18	6.76
Northridge (NP) (Pacoima dam station)	1.580	5.87	5.66	0.32	73.14
Northridge(NR) (scaled) (Rancho station)	0.146	15.45	1.87	0.28	19.65
Northridge (unscaled) (Rancho station)	0.072	5.91	0.70	0.28	7.61
Chi-Chi (Ch) (scaled)	0.146	19.11	5.32	0.34	42.25
Chi-Chi (unscaled)	0.024	3.08	0.84	0.34	7.48

In paper II, four earthquakes have been considered to study the effect of spectrum intensity on response of RC pipe. These are artificial accelerograms corresponding to the Swedish hard rock response spectra [85], and the Eurocode 8 response spectrum for ground type A [29] and accelerograms recorded at Pacoima Dam station during the 1994 Northridge earthquake and accelerograms recorded at LAMONT 1060 station from the 1999 Duzce earthquake [71].

Accelerograms recorded at CDMG 23598 Rancho Cucamonga - Deer Can station during 1994 Northridge earthquake and accelerograms recorded at the ILA004 station during the Chi-Chi (Taiwan) earthquake in 1999 are employed in papers I and III, respectively. The Earthquakes are scaled to have the same PGA with design earthquake of Sweden. Therefore, effects of frequency content of earthquakes on the response of pipelines are studied.

5.3 Finite element models

Dynamic finite element models of soil and pipelines subjected to earthquake excitation have been analysed using the Abaqus/standard finite element software [1]. The simulations are based on two-dimensional (2D) plane strain elements. The models describe two cross-sections of the pipelines; longitudinal and transverse cross-sections. The finite element domain for these cross-sections is shown in **Figures 5.1-5.3**, respectively.

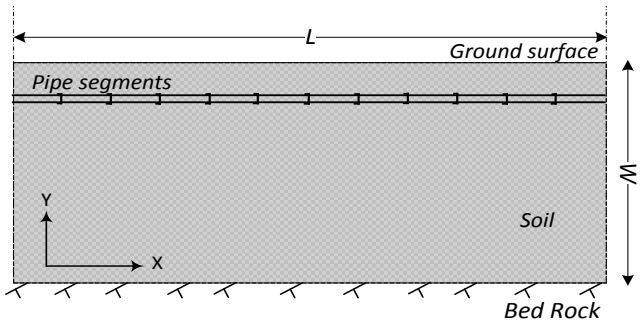

Figure 5.1: Schematic view of finite element domains for longitudinal plane model with uniform ground (model 1)

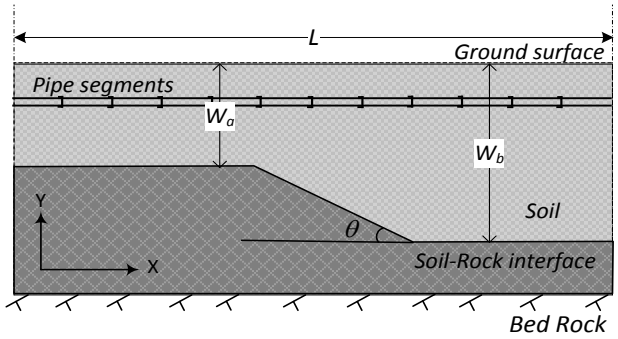

Figure 5.2: Schematic view of finite element domains for longitudinal plane model with non-uniform ground (model 2)

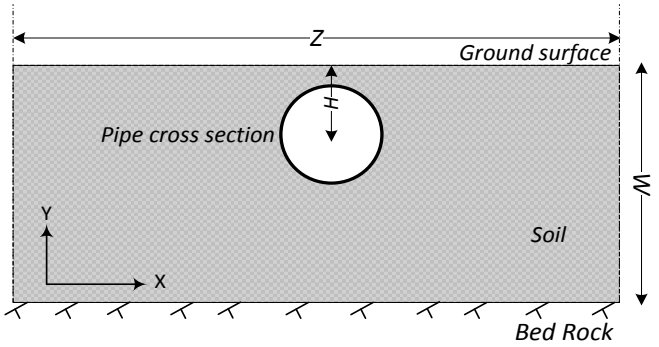

Figure 5.3: Schematic view of finite element domains for cross-section plane model (model 3)

For the longitudinal cross-section, two cases are considered. The first case describes the pipeline buried in uniform ground, see **Figure 5.1** and the second shows the pipeline buried in non-uniform ground caused by inclined bedrock, see **Figure 5.2**. The length of the pipeline has been chosen to capture the longest possible incoming seismic wave length where L=150 m is an adequate length for the analyses. See section 5.4 for a sensitivity analysis of the pipeline length. The relevant soil width Z for the transverse cross-section of the pipe is assumed to be $Z/2 = 3W$, and will be discussed in the following section. Through the aforementioned models effects of burial depth, soil layer thickness, pipeline material, inclined bedrock, water mass, soil type, earthquake frequency content and spectrum intensity are studied within Papers I-III, see **Table 5.3**.

Table 5.3: Model description for parametric study of buried pipelines seismic response.

Parameter	Paper	Model description						
		Model	Pipe type	Rock slope (degree)	Burial depth (m)	Soil depth (m)	Soil type	Earthquake
Burial depth	III	1 and 3	Concrete pipe	0	H =1, H =5	W=25	Ls-Ms-Ds	Se- Ch
Pipe material	-	1 and 3	Concrete pipe, Steel pipe	0	H =1	W =25		Se- Ch
Soil layer thickness	III	1 and 3	Concrete pipe	0	H =1	W =25, W =12	Ls-Ms-Ds	Se- Ch
Inclined bedrock	III	2	Concrete pipe	α=45° α=90°	H =1	W_a=5, W_b=25	Ls-Ms-Ds	Se- Ch
Water mass	I	1,3	Concrete pipe	0	H =1	W =25	Ms-Ds	Se- NR
Spectrum intensity	II	3	Concrete pipe	0	H =1, H =9	W =25	Ms	Se- Eu-Du- NP

5.4 Sensitivity analysis for pipeline length

For dynamic analysis of buried pipelines, it is not practically possible to simulate real length of a long pipeline. On the other hand modelling of a small segment of pipeline cannot give precise result due to the effect of totally neglecting the other parts of pipeline. Therefore, in this study a sensitivity analysis has been done to find a relevent length for the finite element moddeling of the studied pipelines. In this regard four lengths of 75 m, 150 m, 300 m and 600 m have been selected, corresponding to 0.5, 1, 2 and 4 times the largest wave length (predominated wave length) for the studied cases. The analyses are performed for uniform ground with dense soil, which gives the longest possible wave length. The

models have been subjected to the Swedish design earthqauke and Chi-Chi earthquake. **Figures 5.4** and **5.5** show examples of maximum envelopes of tensile stress for axial and bending stresses, respectively. As shown, the maximum stresses occur close to the pipeline ends. In **Figure 5.4**, with increasing pipeline length the maximum axial stress show some convergence until the pipelines with L =300 m and L =600 m reach equal stress levels. With the Swedish earthquake, similar results are obtained. In **Figure 5.5**, for almost all cases the maximum bending stresses occur close to the pipeline ends, but with internal peaks along the pipelines. As seen in this figure, the maximum stresses have converged for L =150 m. For the Chi-Chi earthquake the results are similar, but with a larger number of internal stress peaks, possibly indicating the occurrence of resonance vibrations.

The results from the sensitivity analysis indicate that axial and bending stresses converges at pipeline lengths L between 150 and 300 m. In some cases convergence is evident already at L = 150 m but in other cases it occurs close to L = 300 m. In the latter case, which is twice the 150 m that correspond to the largest wave length, this relationship is such that the results can be due to the signal sampling, which is governed by the Nyquist sampling theorem that specifies that the sampling rate should be twice the highest frequency present in the signal [92]. This needs to be thoroughly investigated in future work, but for the purpose of the numerical work put forth in this thesis pipe lengths of L = 150 m will give adequate precision for the seismic analysis examples that are compared.

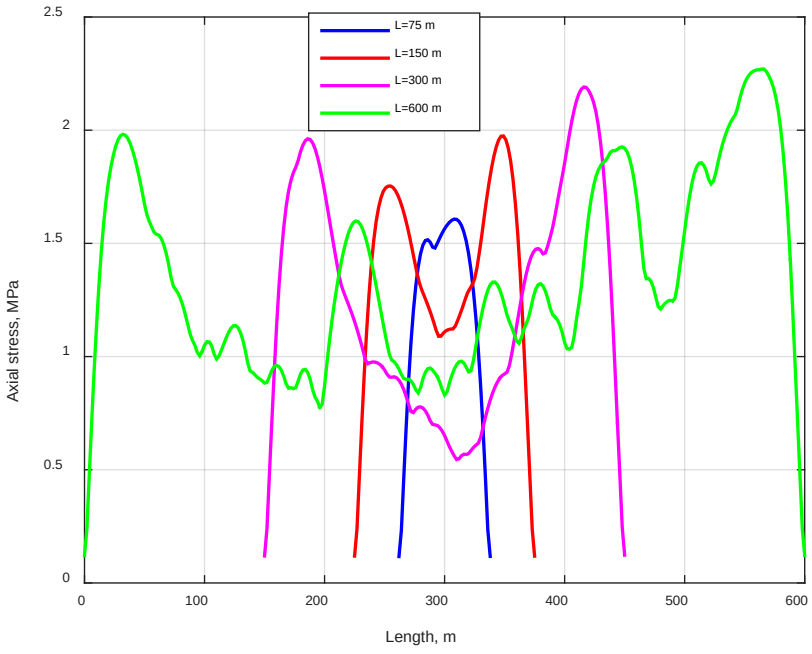

Figure 5.4: Examples of calculated axial stresses for the longitudinal plane section model with varying lengths of pipelines subjected to the Chi-Chi earthquake.

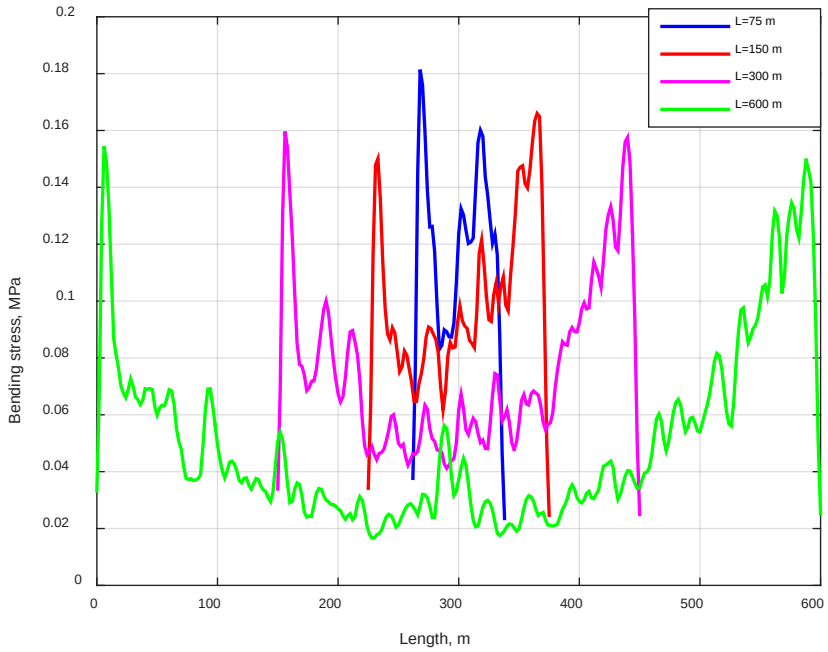

Figure 5.5: Examples of calculated bending stresses for the longitudinal plane section model subjected to the Swedish design earthquake.

5.5 Absorbing boundary condition

In a dynamic soil-structure interaction analysis by the finite element method, the finite computational region is truncated from the infinite space. It is necessary to introduce artificial boundaries to represent both elastic continuity of the soil and radiation damping, otherwise the truncated area must be very large to consider the effect of infinite space and at the same time the finite elements should need be small enough to transmit earthquake waves along the elements, leading to large models which demands too much computational time.

Two kinds of methods are used to set up artificial, global and local procedures. The former are rigorous, but complex and computationally expensive (e.g. boundary element method, scaled boundary finite element method). The latter are generally approximate, but simple. They have been widely used in civil engineering, e.g. for viscous boundaries and infinite elements. In order to obtain accurate results, local artificial boundaries have to be placed sufficiently far away from the structure-soil interface [9]. Herein three types of local boundaries that commonly are used in dynamic finite element modelling of soil-structure interaction, are compared in order to find the most relevant one. These are viscous boundary, viscous spring boundary and infinite elements. The viscous boundary was proposed by Lysmer and Kuhlemeyer [59], and consists of normal and tangential dampers on each node of boundary with coefficients C_n and C_t, respectively.

$$C_n = A.a.\rho.v_p \tag{5.1}$$

$$C_t = A.b.\rho.v_s \tag{5.2}$$

where *A* is the total area of all elements around the node considered on the boundary, *a* and *b* are dimensionless parameters, v_s is the shear wave velocity and v_p the compression wave velocity.

$$v_s = \sqrt{G/\rho} \tag{5.3}$$

$$G = E/2(1+\upsilon) \tag{5.4}$$

$$V_p = \sqrt{(\lambda + 2G)/\rho} \tag{5.5}$$

$$\lambda = \frac{E\upsilon}{(1+\upsilon)(1-2\upsilon)} \tag{5.6}$$

where *G* is shear modulus, *E* is Young's modulus, υ is Poisson's ratio, ρ is mass density and λ is the Lame's constant. It was found that for *a*=*b*=1, good absorption will take place. To simulate this boundary in ABAQUS [1] a dashpot element DASHPOT1 has been used.

The viscous spring boundary was presented by Deeks and Randolph [23], for the plain strain case based on cylindrical wave theory. Then, Liu et al. [58], developed 3D viscous spring boundaries using spherical wave theory. The viscous spring boundaries use spring elements to represent soil continuity and static equilibrium, and dashpot elements to absorb scattering wave energy that would reach the boundary if the spring elements were cancelled. The viscous spring boundary consists of normal and tangential linear springs and dashpots with the following coefficient for two-dimensional and three-dimensional spaces, respectively. Coefficients for two-dimensional spaces are:

$$K_n = A.\frac{2G}{R}, \quad C_n = A.\rho.v_p \tag{5.7}$$

$$K_t = A.\frac{G}{2R}, \quad C_t = A.\rho.v_s \tag{5.8}$$

Coefficients for three-dimensional spaces are:

$$K_n = A.\frac{4G}{R}, \quad C_n = A.\rho.v_p \tag{5.9}$$

$$K_t = A.\frac{2G}{R}, \quad C_t = A.\rho.v_s \tag{5.10}$$

Where A is the total area of all elements around node considered on the boundary and R is the shortest distance between wave source and plane of the boundary. To simulate viscous spring boundary in ABAQUS a spring element SPRING1 and dashpot element DASHPOT1 has been used.

The infinite element boundary provided by ABAQUS [1], is based on the work of Zienkiewicz et al. [96] for static response and of Lysmer and Kuhlemeyer [59] for dynamic response. Therefore, the infinite element boundary is a kind of implementation of the viscous boundary to absorb the energy in a dynamic analysis. An infinite element is a linear element which only can have linear behaviour. One important point about these elements is about node numbering which element edges do not cross over in the infinite direction. For two-dimensional problems ABAQUS provides two types of infinite elements; CINPS4 and CINPE4 for plane stress and plain strain analysis which is supported with both ABAQUS/Explicit and ABAQUS/Standard.

In order to investigate the relationship between soil width Z and soil depth W (see **Figure 5.3**) and the type of boundary condition used, three examples have been considered with $Z/2=W$, $Z/2=2W$ and $Z/2=3W$, for the pipe with 9 m burial depth subjected to the Swedish design earthquake. An observation point was selected at the crown of the pipe. The x-direction displacement time history at the observation point for three types of boundaries has been compared. **Figure 5.6** indicates the x-direction displacement time history for a fixed distance of $Z/2=W$ for different boundaries. It can be seen that the three boundaries have different displacement time histories, especially at 10 sec in which for Lysmer type and infinite element boundaries the displacement does not converge to zero. In these cases, the model is like a separated body floating in the air, which can drift under low frequency loads. For $Z/2=2W$, the displacement time histories for all boundaries are almost the same between 0 and 8 sec, but after 8 sec Lysmer and viscous spring boundaries do not converge to zero, see **Figure 5.7**. For $Z/2=3W$, the displacement time histories for all boundaries converge to zero, see **Figure 5.8**. The convergence analysis indicates that the distance $Z/2=3W$ is a good approximation for placing the artificial boundaries. Among the three absorbing boundaries, infinite element boundary has better performance at low frequency loads.

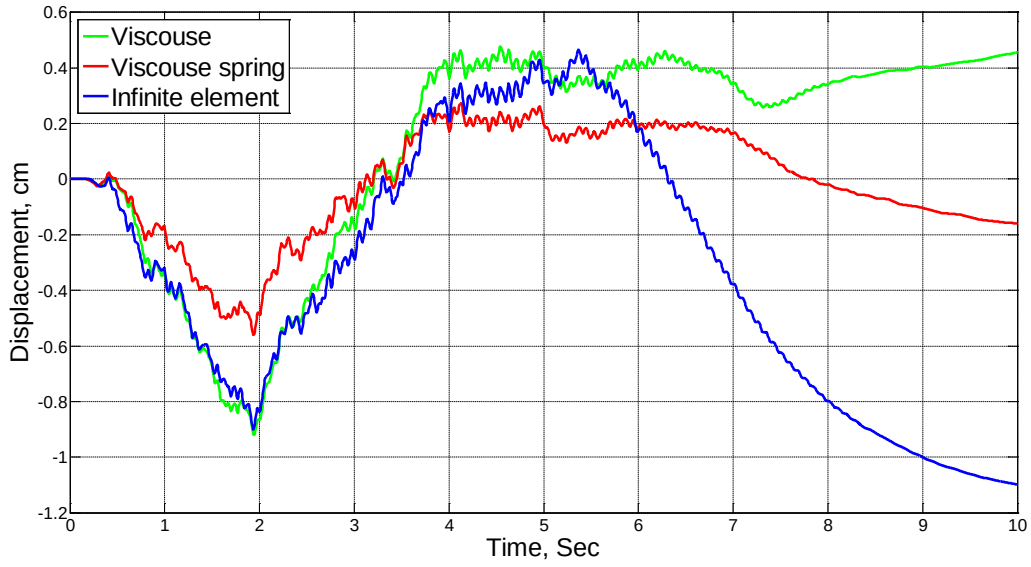

Figure 5.6: The *x*-direction displacement time history at observation point with fixed distance $Z/2=W$ for different boundaries.

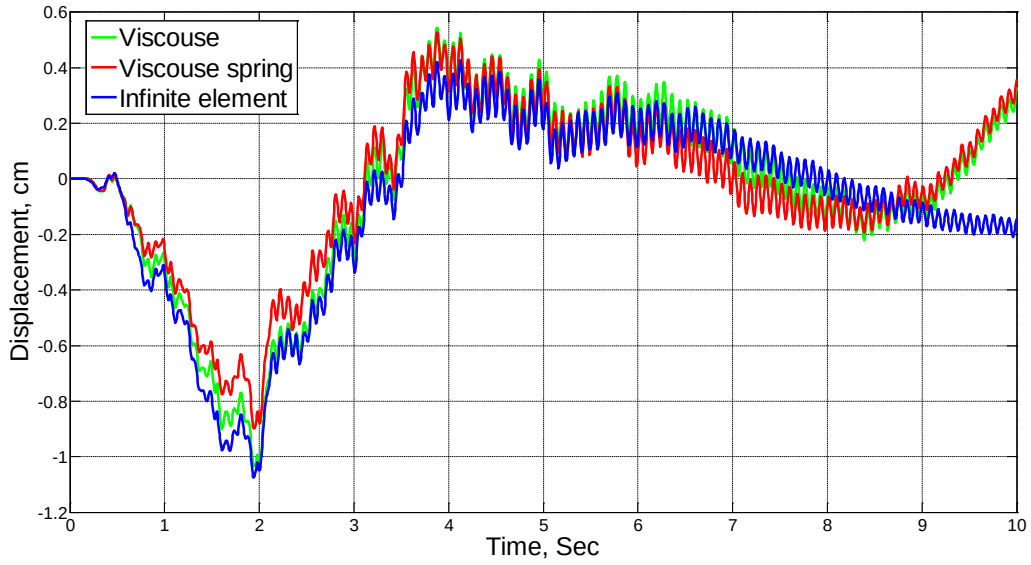

Figure 5.7: The *x* -direction displacement time history at observation point with fixed distance $Z/2=2W$ for different boundaries.

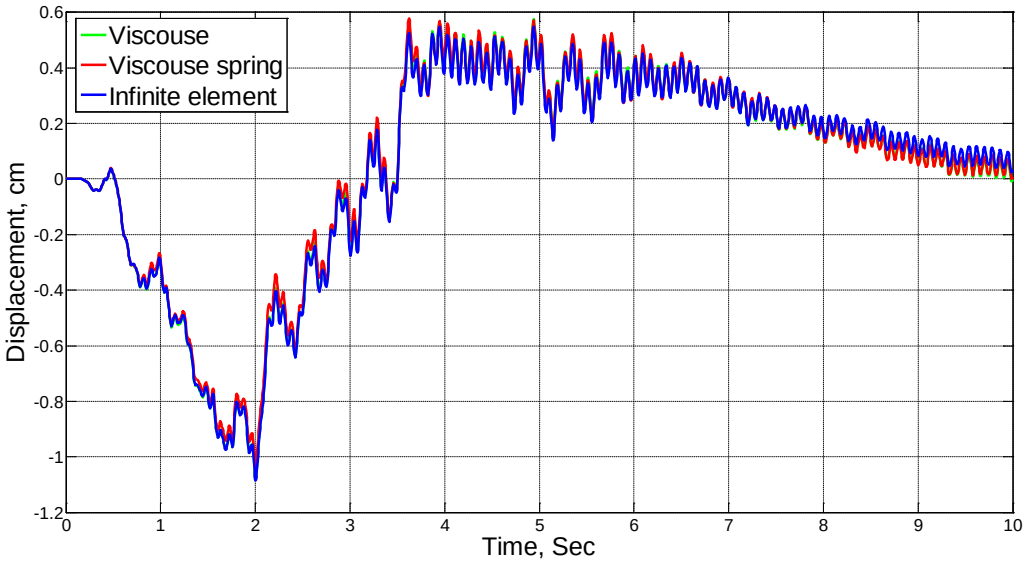

Figure 5.8: The *x*- direction displacement time history at observation point with fixed distance *Z*/2=3*W* for different boundaries.

5.6 Damping

For seismic analysis of soil-pipe systems with linear materials, it is desirable to define material damping as a dissipation source. There are two different methods for defining damping in such a system; Modal damping and Rayleigh damping. Rayleigh damping is applicable in direct-integration dynamic analyses which defines a mass and stiffness proportional damping ratio for the *i*th mode described with the following equation:

$$\xi_i = \frac{\alpha}{2.\omega_i} + \frac{\beta.\omega_i}{2} \tag{5.11}$$

where α and β are a mass damping coefficient and a stiffness damping coefficient, respectively. This equation produces a curve which is a function of the circular natural frequency of the *i*-th mode $\omega_i = 2\pi f$ [15]. In this project a modal damping for materials that is 5% has been assumed. For example, the model in paper II has a Rayleigh damping such as seen in **Figure 5.9**.

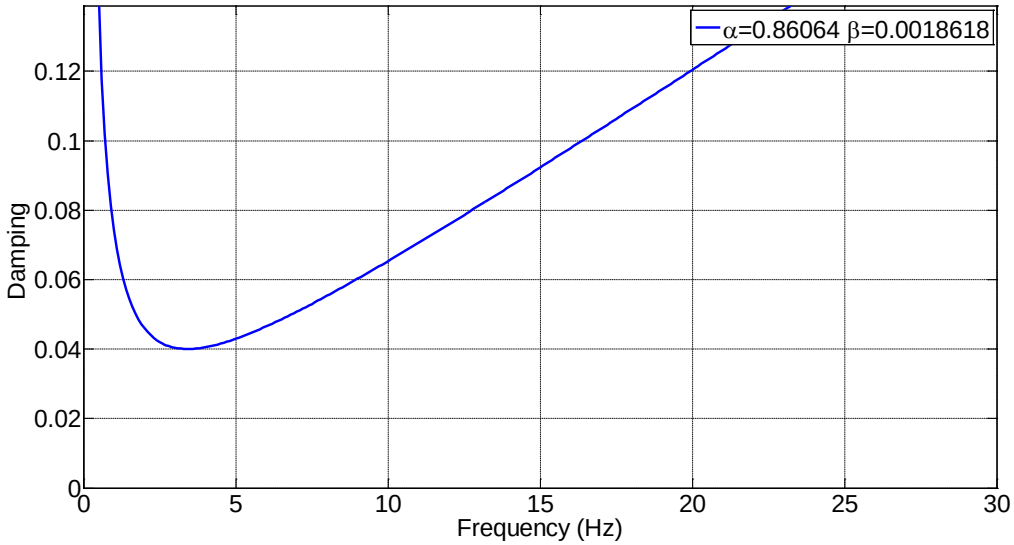

Figure 5.9: Rayleigh damping for model 3, described in paper II.

5.7 Finite element analysis

The described finite element models in section 5.3 are discretized with 4-node bilinear plane strain quadrilateral (CPE4R) elements for the soil medium and pipe cross-section, 3-node quadratic 2D truss (T2D3) elements for the reinforcement and 2-node linear 2D beam (B21) elements for the longitudinal cross-sections of pipelines. A fine mesh is used around soil-pipe interfaces and coarser mesh away from pipe-soil interfaces. The interaction between reinforcement and concrete elements is assumed as fully bonded. The soil-pipe interaction is modelled with SPRING2 elements at the soil-pipe interface. The behaviour of the springs is calculated using formulas by the American Lifeline Alliance (ALA), see section 4.3. Infinite elements (CINPE4) have been placed at lateral boundaries. The Rayleigh damping is used with α and β coefficients to attenuate the internal energy generated from seismic loading. The earthquake excitation is applied as an acceleration boundary condition at the base of the models. Before performing dynamic analysis, frequency analysis is done to identify natural frequencies of the mechanical systems and effective modal mass (see Paper I) of each mode. These characterizes can be shown by the cumulative effective modal mass which indicates the natural frequency and vibration modes that significantly contribute to the vibrations.

CHAPTER 6

Numerical Results

In this study first, frequency analyses are done to investigate the mechanical properties of the FE models, and then the models are subjected to earthquakes with different frequency contents in order to study the dynamic response. Results from frequency analysis are shown by cumulative effective mass for horizontal direction and vertical direction of models. Dynamic response of pipelines is described in terms of maximum tensile stress which is an important key parameter for concrete structures. The maximum tensile stress is here presented as stress envelopes, the maximum stress at each section of the length and cross-section of pipelines reached during the analysis time span. For the longitudinal plane section model, maximum axial tensile stress and maximum bending tensile stress are calculated. For the transverse cross-section model, maximum principal tensile stress is calculated. The location of maximum principal stresses in the circular plane section of the pipelines are described by polar angles, positive in the clockwise direction and originating from the crown of the pipelines. In the following sections some examples from Papers I-II-III are summarized and commented. Further examples and backgrounds are given in these papers. Additional examples are also given here; amongst others are the stress responses in steel pipelines shown for comparison with the results for concrete pipelines.

6.1 Effective modal mass

Figure 6.1(a) shows cumulative effective modal mass for the longitudinal plane section model with 25 m soil layer thickness. As shown in this figure high stiffness soil has higher frequency content. A decrease in soil layer thickness changes cumulative effective modal mass of model such as in **Figure 6.1(b)** in which the predominated frequency for soil layer thickness equal to 12 m is almost twice as for the one with 25 m soil layer thickness. **Figure 6.1(c)** illustrates cumulative effective modal mass for the longitudinal plane section model with inclined bedrock with α=45° which compared to uniform ground has higher frequencies.

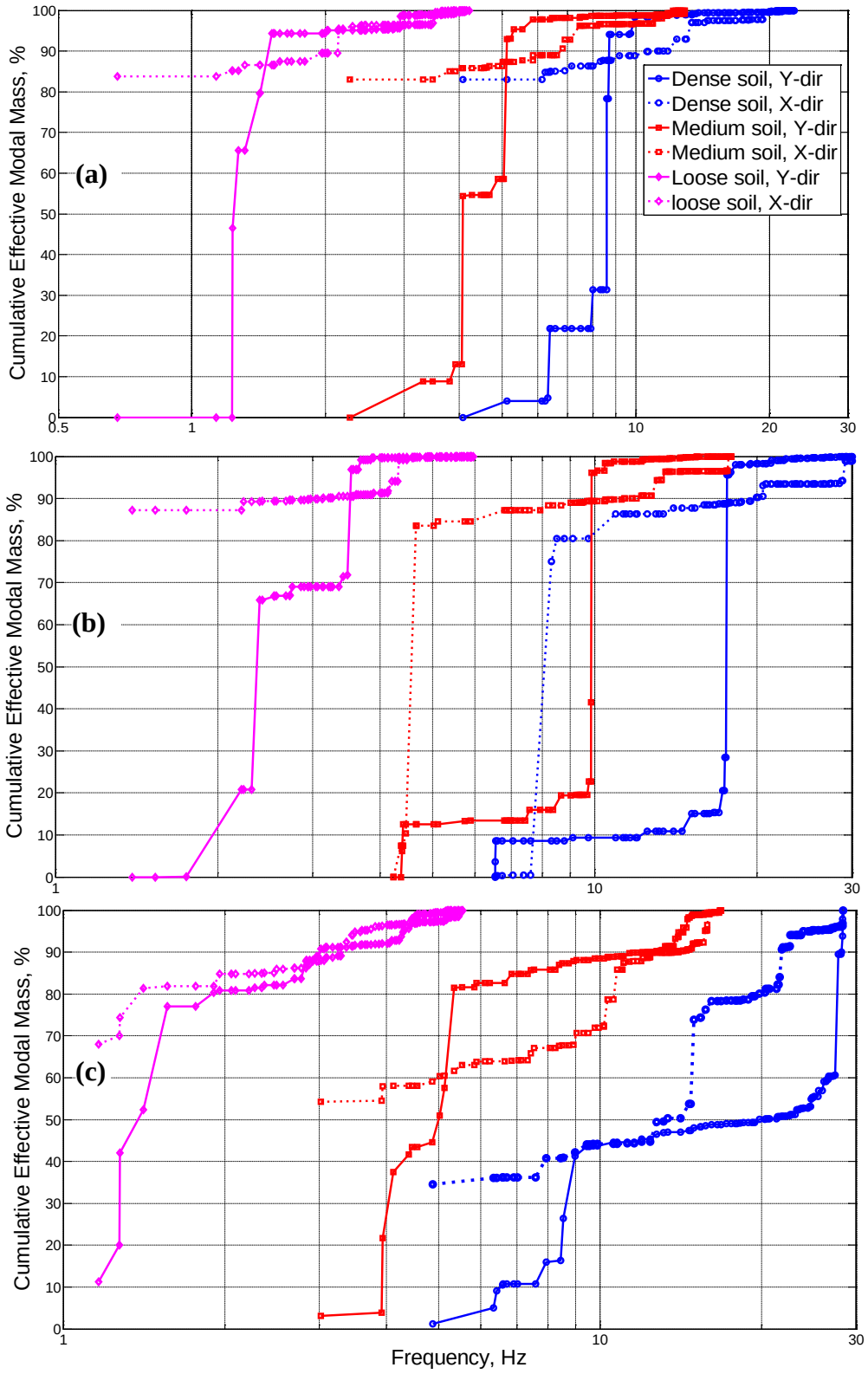

Figure 6.1: Cumulative effective modal mass for the longitudinal plane section model, with 25 m soil layer thickness (a), 12 m soil layer thickness (b), inclined bedrock with α=45° (c) [Paper I**,** III].

6.2 Response of reinforced concrete pipelines - water mass effect

The effect of water mass has been investigated in Paper I. **Figure 6.2** and **6.3** show the maximum axial tensile stress and the maximum bending tensile stress induced in pipelines due to Northridge earthquake. Each figure contains four curves representing the combinations of the cases with empty or water filled pipelines and dense or medium hard surrounding soil, respectively. It is observed that water mass has slight effect on axial tensile stress of pipelines, while its effect is significant for bending tensile stress of pipeline in medium stiffness soil.

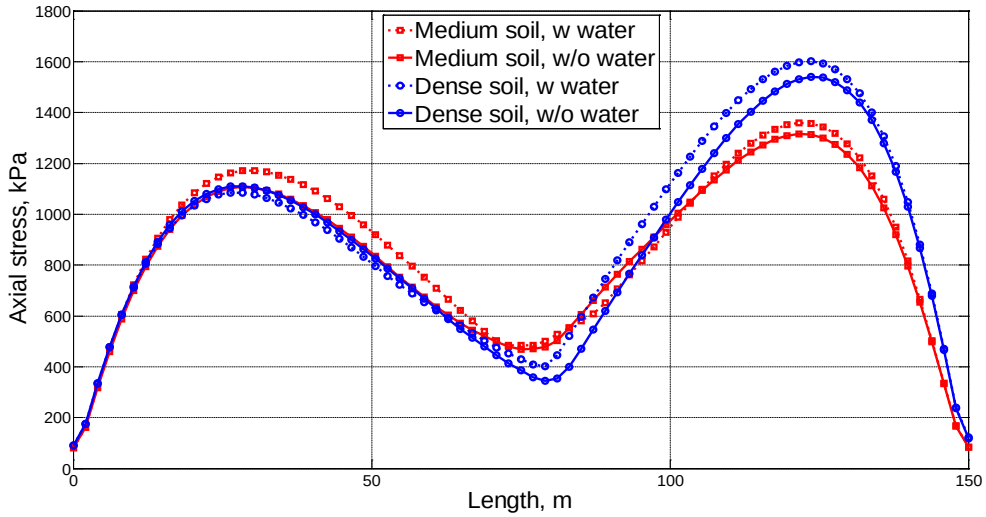

Figure 6.2: Axial stress for the longitudinal plane section model subjected to the Northridge earthquake [Paper I].

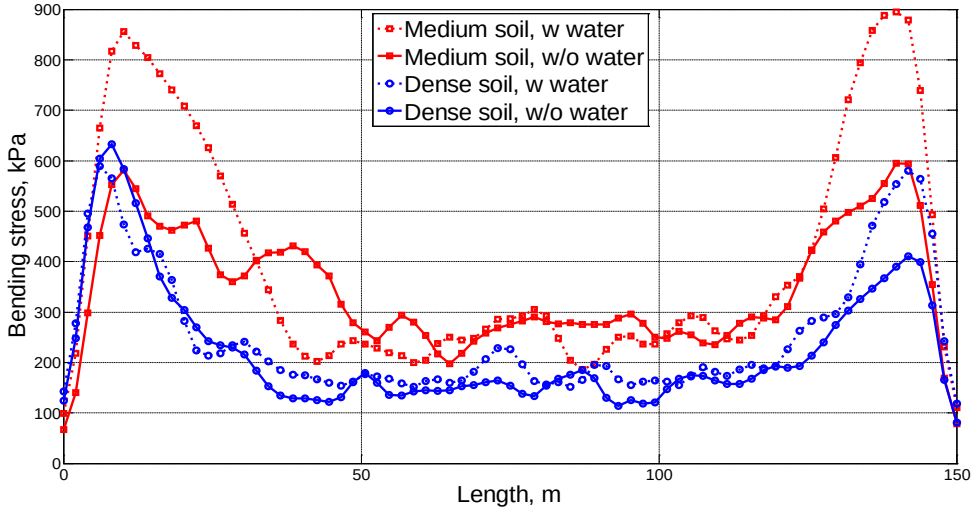

Figure 6.3: Bending stress for the longitudinal plane section model subjected to the Northridge earthquake [Paper I].

6.3 Response of reinforced concrete pipelines from burial depth effect

Figures 6.4 and **6.5** illustrate maximum axial tensile stress for the longitudinal plane section model induced by the Swedish design earthquake and the Chi-Chi earthquake, respectively. **Figure 6.6** shows maximum bending stress for the longitudinal plane section model from the Swedish design earthquake and the Chi-Chi earthquake, respectively. The figures show a comparison between shallowly buried pipelines, *H*=1 m and deeply buried pipelines, *H*=5 m [Paper III]. As observed an increase in the burial depth leads to increase the maximum axial tensile stress for dense and medium stiffness soil but for loose soil, the changes is not significant. For bending stress, maximum tensile strength for dense soil is decreased but for medium and loose soil, maximum tensile stress is increased. **Figure 6.7** shows maximum principal stress based on Eurocode 8 and the Duzce earthquake, for pipelines buried in medium stiff soil at 1 and 9 m distance from the ground surface [Paper II]. Maximum tensile stress through concrete thickness and reinforcement has been shown separately in which an increase in burial depth but also in earthquake intensity leads to an increased tensile ring stresses.

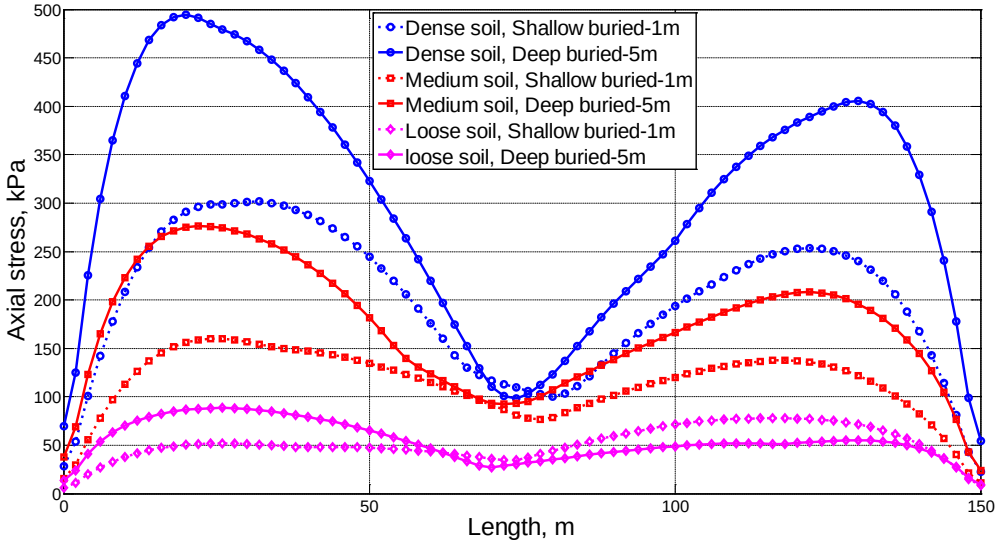

Figure 6.4: Maximum axial stress for the longitudinal plane section model from the Swedish design earthquake [Paper I**,** III].

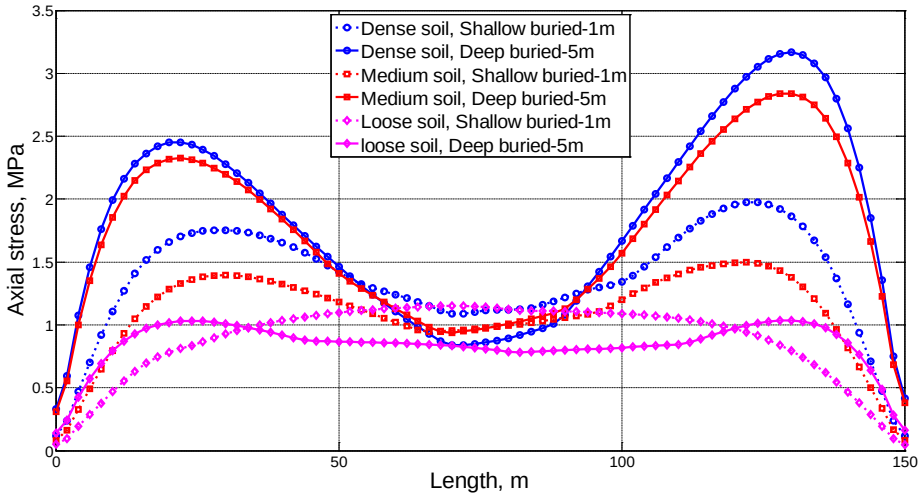

Figure 6.5: Maximum axial stress for the longitudinal plane section model from the Chi-Chi earthquake [Paper III].

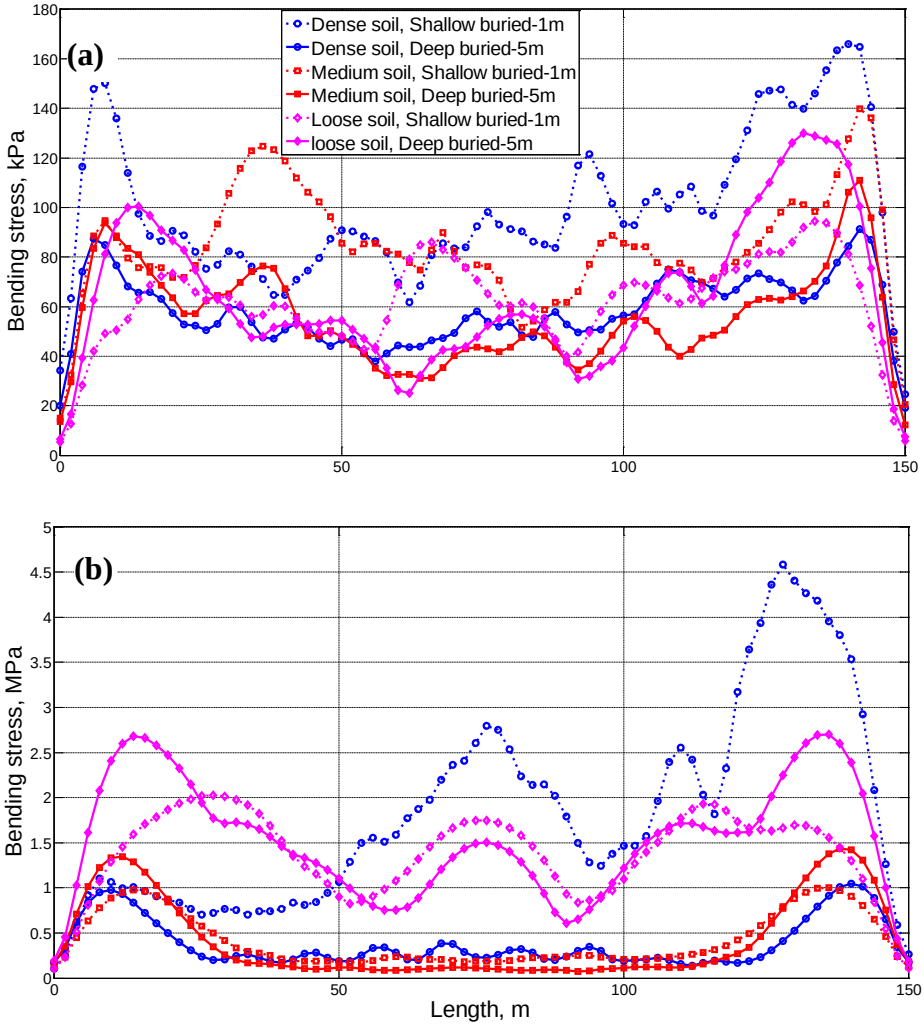

Figure 6.6: Maximum bending stress for the longitudinal plane section model, from the Swedish design earthquake [Paper I**,** III] (a) and the Chi-Chi earthquake (b) [Paper III].

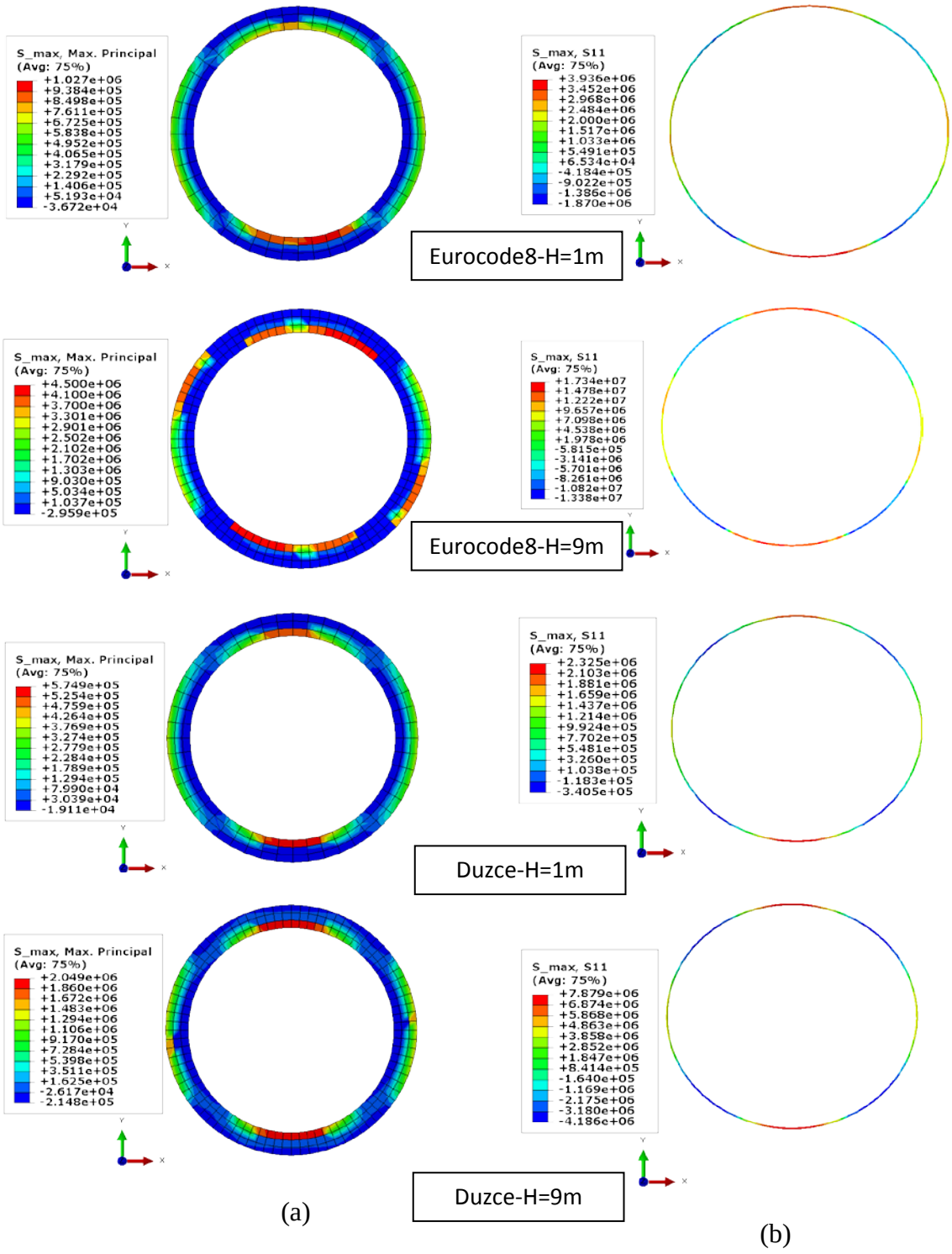

Figure 6.7: Maximum tensile stress in transverse cross-section of reinforced concrete pipe due to Eurocode8 and the Duzce earthquakes for 1 and 9 m burial depth and medium stiffness soil; a) Maximum principal stress through concrete pipe thickness and b) Ring stress along reinforcement [Paper II].

6.4 Response of reinforced concrete pipelines from soil layer thickness effect

The effect of soil layer thickness has been studied in Paper III. **Figures 6.8 and 6.9** illustrate maximum axial stress and maximum bending stress induced by the Swedish design earthquake for the longitudinal plane section model of pipelines located at 1 m from ground surface, respectively. As observed from figures, for axial tensile stress, larger soil layer thickness gives higher axial stress. While for bending tensile stress, a decreased soil layer thickness leads to increased bending tensile stress.

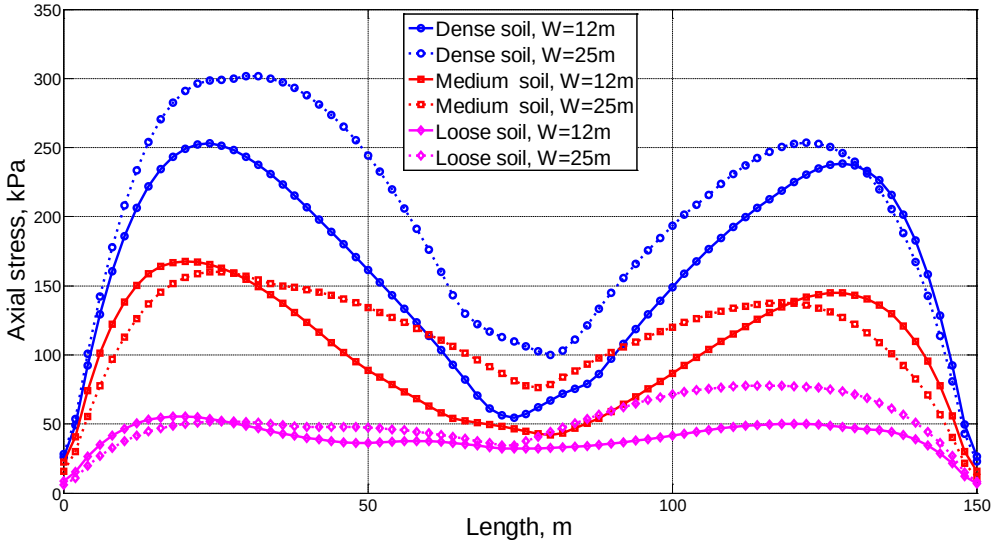

Figure 6.8: Maximum axial stress for the longitudinal plane section model with *H*=1m subjected to the Swedish design earthquake [Paper III].

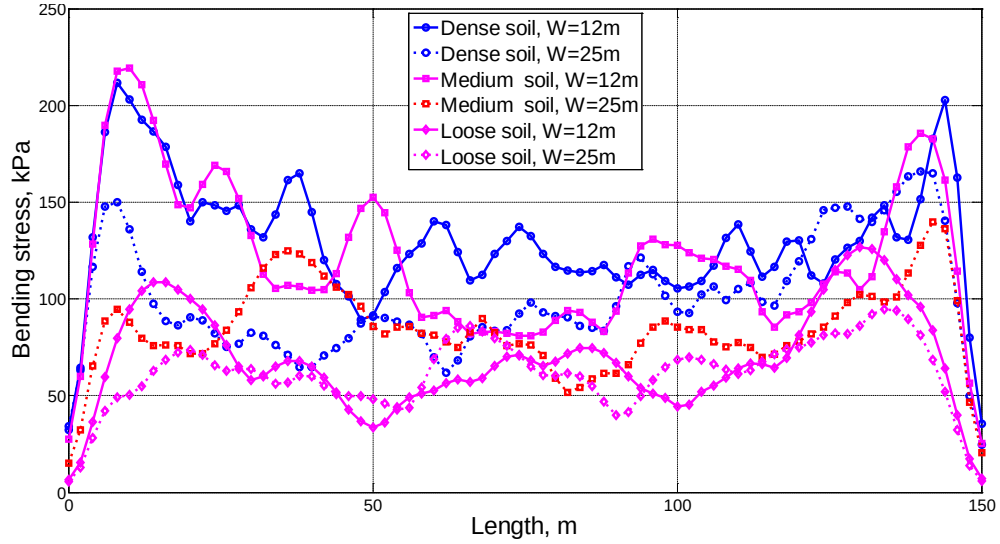

Figure 6.9: Maximum bending stress for the longitudinal plane section model with *H*=1m subjected to the Swedish design earthquake [Paper III].

6.5 Response of reinforced concrete pipelines from non-uniform ground effect

The effect of non-uniform ground caused by inclined bedrock has been investigated in Paper III. **Figures 6.10** and **6.11** show maximum axial tensile stresses for the longitudinal plane section model with inclined bedrock subjected to the Swedish design earthquake and the Chi-Chi earthquake, respectively. **Figure 6.12** illustrates maximum bending tensile stresses for the longitudinal plane section model with inclined bedrock subjected to the Swedish design earthquake and the Chi-Chi earthquake, respectively. As observed in these figures, small differences exist in tensile stress for inclined angle 45 degree and 90 degree for each type of soil. A comparison between these figures and tensile stress for uniform ground, see stress for shallowly buried pipelines in **Figure 6.4-6.6**, shows a significant increase in tensile stress due to inclined bedrock. **Figure 6.13** shows the maximum axial sectional force and maximum sectional moment along longitudinal the cross-section of pipelines due to the Swedish design earthquake, for models with uniform and non-uniform ground [Paper I - III]. It can be seen that model with inclined bedrock has higher axial sectional force and sectional moment where the maxima are located at centre part and right part of the pipeline which corresponds to the inclined part of the bedrock and larger soil layer thickness, respectively.

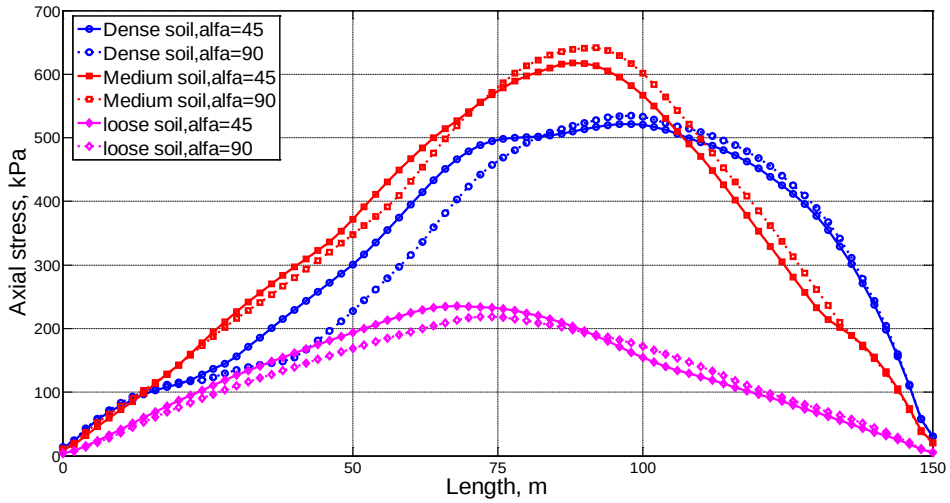

Figure 6.10: Effect of inclined bedrock on axial stress for the longitudinal plane section model subjected to the Swedish design earthquake [Paper III].

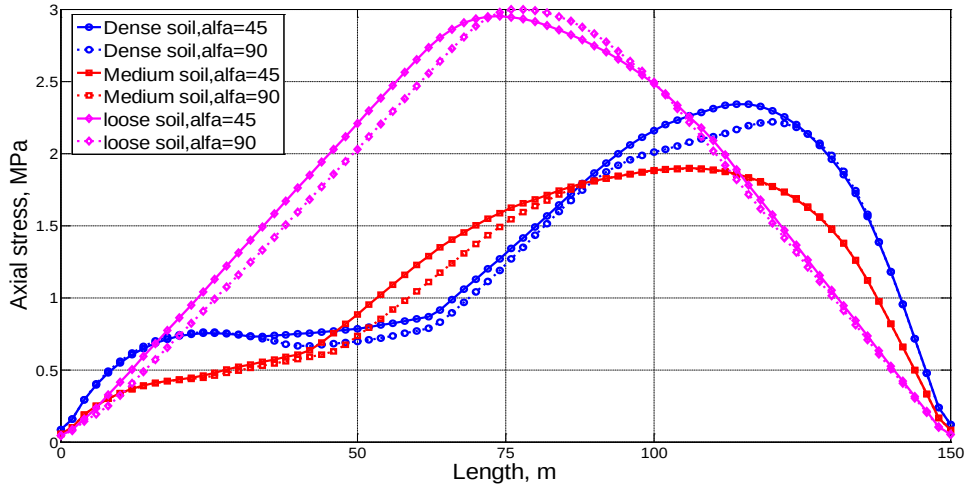

Figure 6.11: Effect of inclined bedrock on axial stress for the longitudinal plane section model subjected to the Chi-Chi earthquake [Paper III].

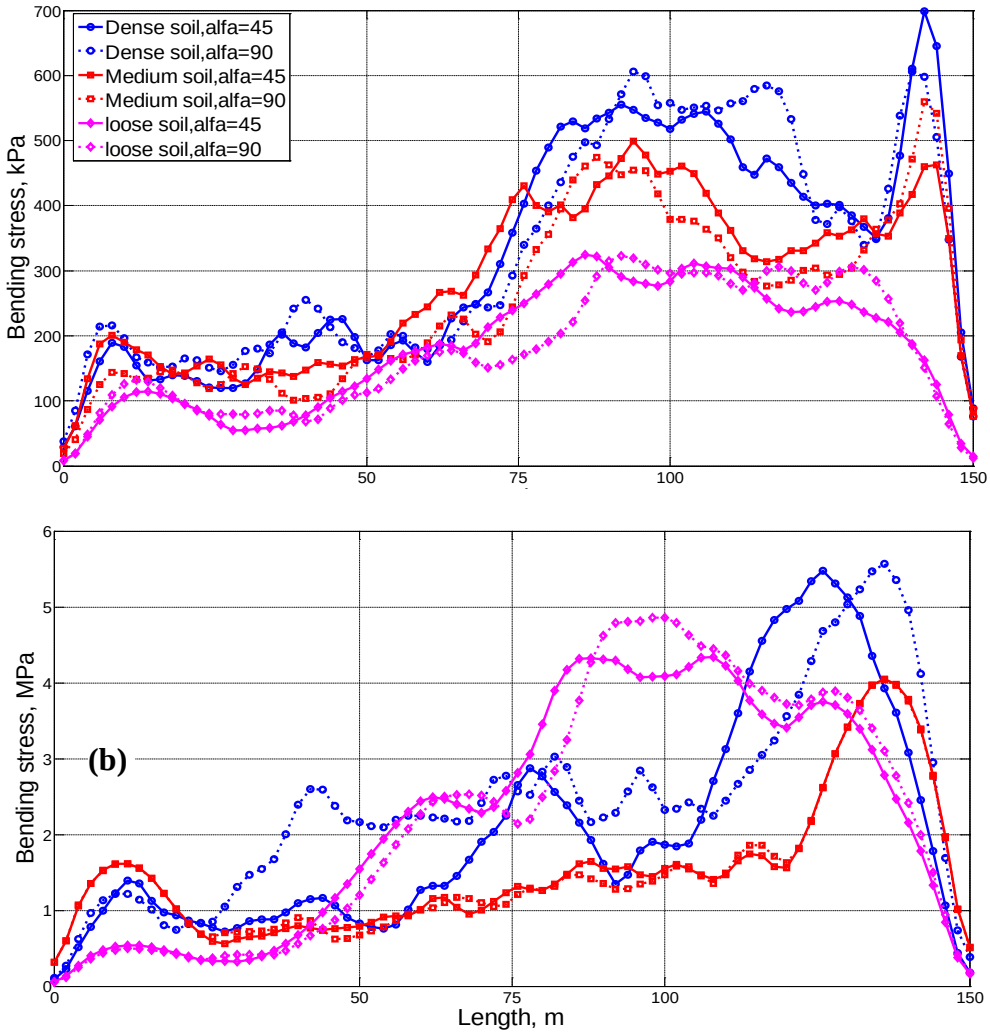

Figure 6.12: Effect of inclined bedrock on bending stress for the longitudinal plane section model, subjected to the Swedish design earthquake (a) and the Chi-Chi earthquake (b) [Paper III].

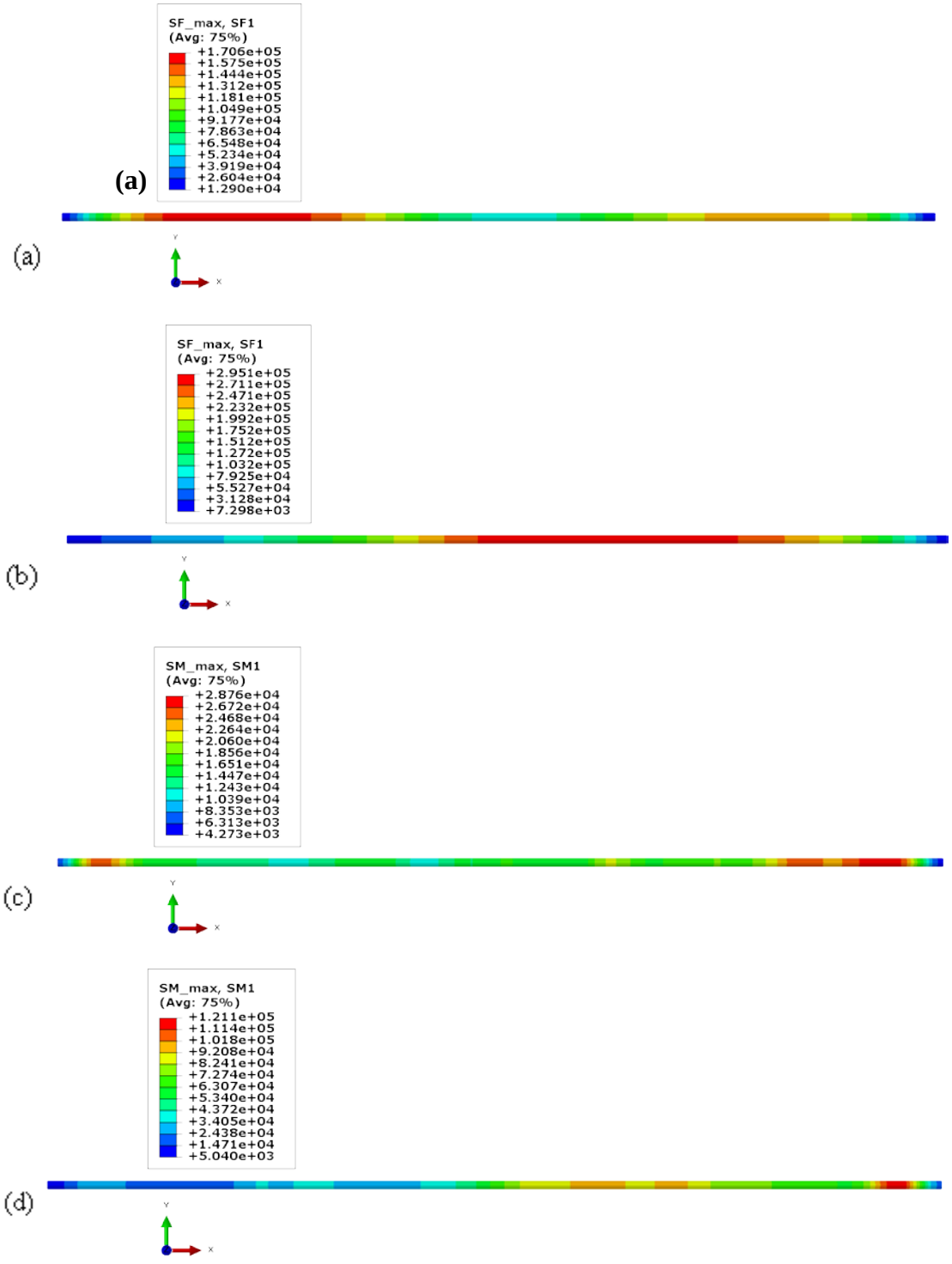

Figure 6.13: Maximum tensile stress for longitudinal cross-section of pipe subjected to design earthquake of Sweden with 1 m burial depth and dense stiffness soil; a and b) Maximum axial sectional force for uniform and non-uniform ground, respectively, c and d) Maximum sectional moment for uniform and non-uniform ground, respectively [Paper I**,** III].

6.6 Response of buried steel pipelines

In the preceding sections the response of concrete pipelines as a rigid material was described. In this section, the response of steel pipelines as a flexible material is studied. For this purpose, dynamic analysis has been performed for a model with 25 m soil layer thickness and 1 m burial depth excited by the Swedish design earthquake and the Chi-Chi earthquake. **Figures 6.14-6.16** show the dynamic response of steel pipelines. Each figure includes two subfigures (a) and (b) for dynamic response of steel pipelines due to the Swedish designs earthquake and the Chi-Chi earthquake, respectively. **Figure 6.14** shows maximum axial stress in steel pipelines for the longitudinal plane section model. The maximum bending stress in longitudinal plane section model and maximum principal stress for transverse cross-section model is illustrated in **Figure 6.15** and **Figure 6.16**, respectively. Maximum axial tensile stresses induced by the Swedish design earthquake for dense soil, medium soil and loose soil are 2.4 MPa, 1.5 MPa and 1 MPa, respectively, see **Figure 6.14(a)**. For the Chi-Chi earthquake, see **Figure 6.14(b),** there are small differences in the maximum axial tensile stress levels, which all peaks are between 12-14 MPa. The only difference is that for loose soil there is one peak at the centre of the pipe while the two other soil types result in two peaks.

For bending stresses induced by the Swedish design earthquake, there are small differences in tensile bending stress for the three types of soils, with a maximum tensile stress that is almost equal to 600 kPa, see **Figure 6.15(a).** For bending tensile stresses induced by the Chi-Chi earthquake, see **Figure 6.15(b),** loose soil gives a higher bending stress equal to 11 MPa, whereas for medium and dense soils, the maximum stress is 6.2 MPa and 5.0 MPa, respectively. The maximum ring tensile stress induced by the Swedish design earthquake is 10 kPa for dense soil see **Figure 6.16(a)**. For the Chi-Chi earthquake, maximum ring tensile stress is 52 kPa which belongs to medium soil, see **Figure 6.16(b)**.

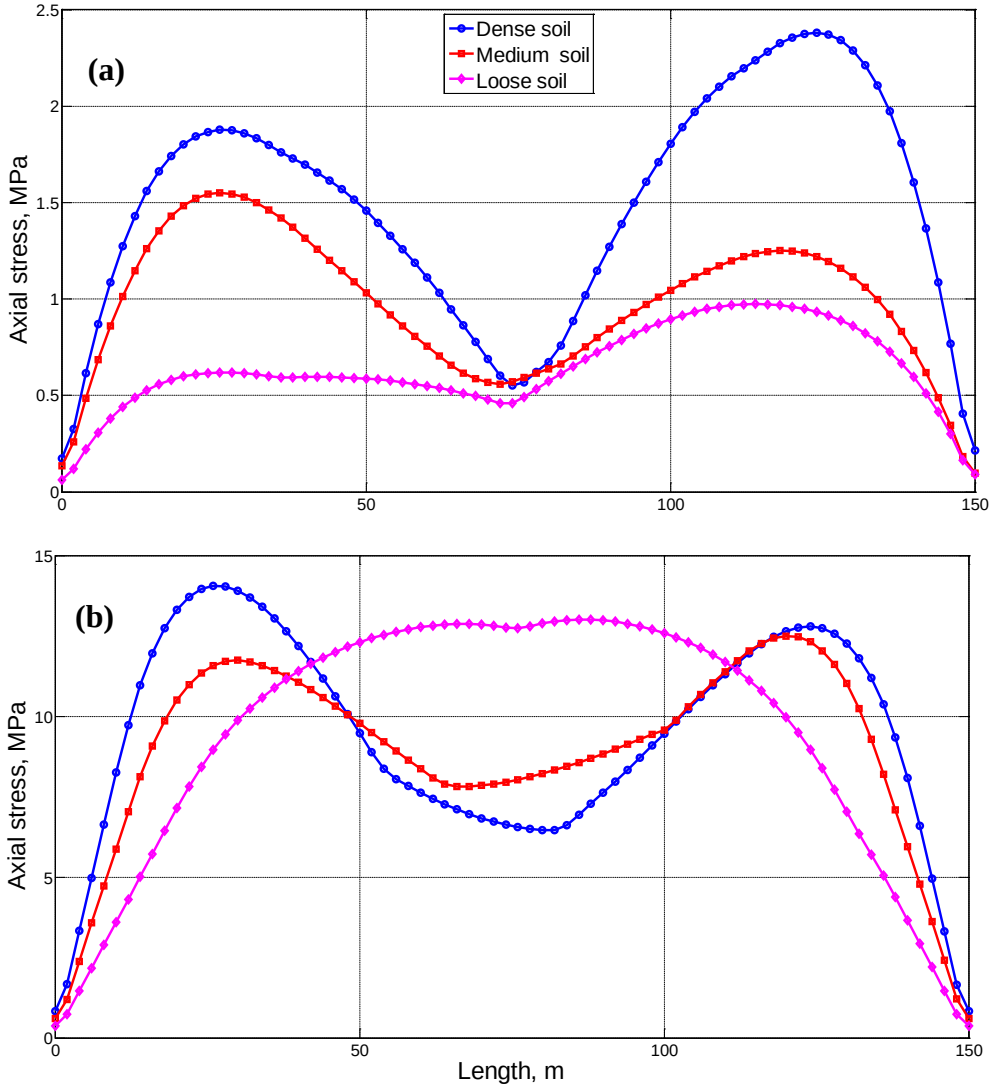

Figure 6.14: Maximum axial stress in steel pipelines for the longitudinal plane section model, from the Swedish design earthquake (a) and the Chi-Chi earthquake (b).

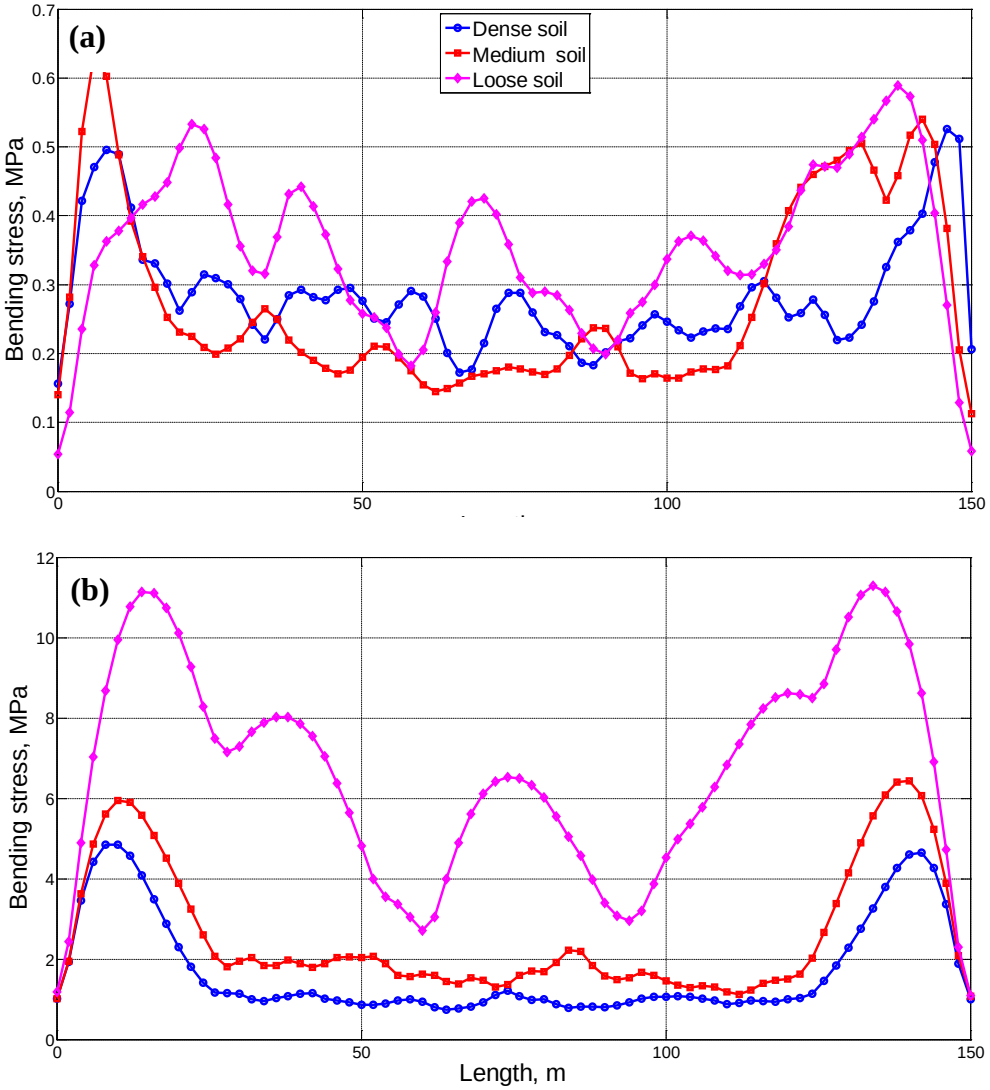

Figure 6.15: Maximum bending stress in steel pipelines for the longitudinal plane section model, from the Swedish design earthquake (a) and the Chi-Chi earthquake (b).

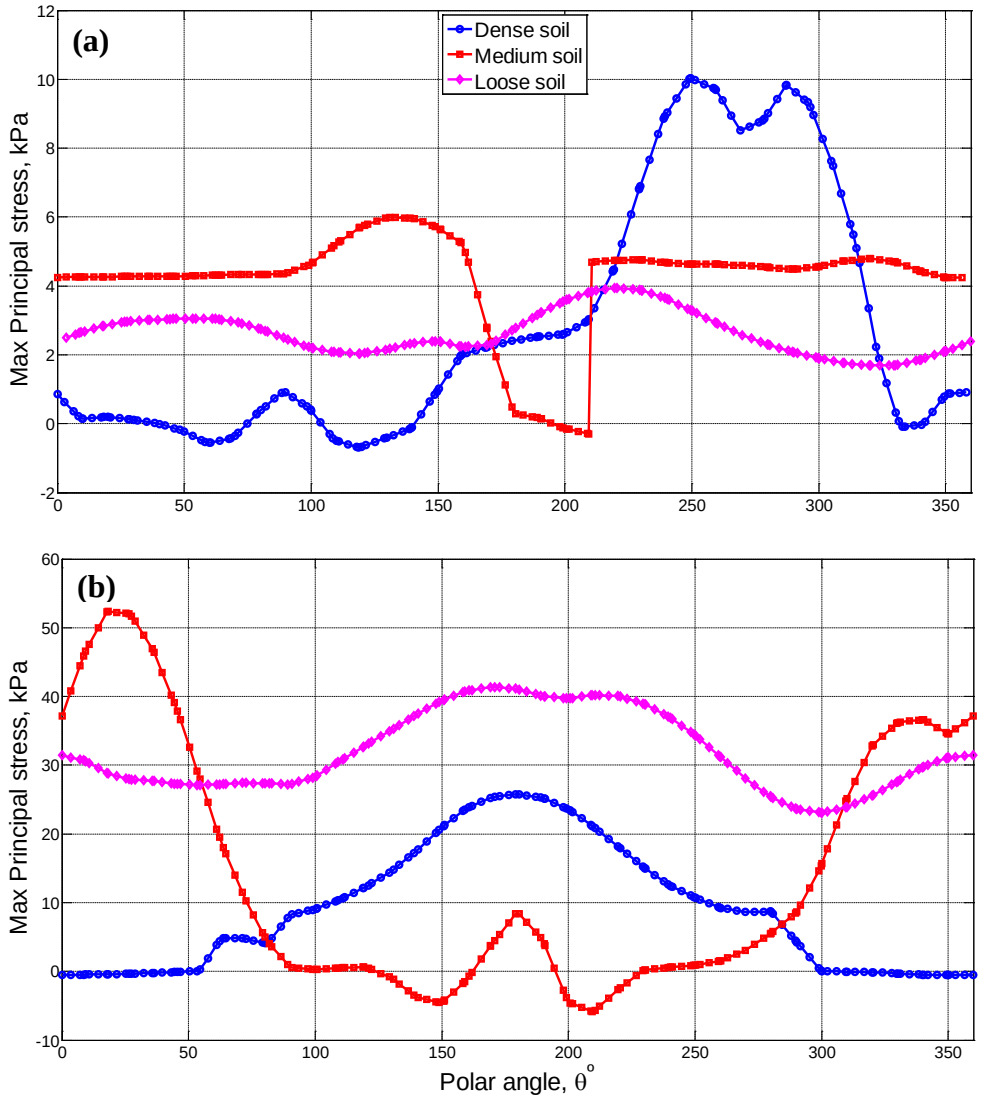

Figure 6.16: Maximum principal stress in steel pipelines for the cross-section plane model, from the Swedish design earthquake (a) and the Chi-Chi earthquake (b).

CHAPTER 7

Conclusions

In this project finite element models have been developed to study the response of reinforced concrete pipelines due to high-frequency excitation, but also low-frequency excitations for comparison purposes. The effects of burial depth, soil layer thickness, water mass, non-uniform ground caused by inclined bedrock, earthquake intensity and piping material have been studied. In this chapter, the results obtained from these effects are first discussed. Then, general conclusions and future work are presented.

7.1 Discussion

The effect of water mass has been investigated for shallowly buried concrete pipelines in Paper I. In the paper, dynamic analyses are performed for dense soil and medium dense soil subjected to ground accelerations similar to the Swedish design earthquake and the Northridge earthquake, see Table 7.1. The results show slight differences between axial tensile stresses in water filled and empty pipelines. The maximum axial tensile stress due to Swedish design earthquake has a value of 320 kPa for dense soil, while for the Northridge case, the maximum tensile stress is between 1400-1600 kPa. Water mass has a significant effect on the bending tensile stress. For the Northridge earthquake, the effect is larger for medium dense soil in which the maximum bending tensile stress for a case with empty and water filled pipes are 600 kPa and 900 kPa, respectively and 150 kPa and 320 kPa for the Swedish design earthquake and dense soil. For ring stresses induced by the Swedish design earthquake, including water mass increases the maximum tensile stress with dense soil, from 55 kPa to 110 kPa. For the Northridge earthquake, different behaviour is seen for medium dense and dense soils. For medium dense soil adding water mass increases the maximum tensile stress from 40 kPa to 62 kPa, while for dense soil it decreases the maximum tensile stress from 4 MPa to 2.5 MPa.

Table 7.1: Maximum tensile stress induced in concrete pipelines (Paper I).

Soil type		Axial stress, kPa		Bending stress, kPa		Ring stress, kPa	
		Sweden	Northridge	Sweden	Northridge	Sweden	Northridge
With water	Medium soil	150	1350	190	900	58	62
	Dense soil	320	1300	320	600	110	2500
Without water	Medium soil	155	1600	120	600	55	40
	Dense soil	300	1550	150	610	55	4000

In Paper II, the relationship between earthquake spectrum intensity and maximum ring stresses in reinforced pipelines has been studied. The analysis was done for medium dense soil with shallow and deep burial depths equal to 1 m and 9 m, respectively. Four earthquakes have been selected with spectrum intensities in the range of 3-75 cm/sec, see Table 7.2. The results show that the maximum tensile stress is directly proportional to the spectrum intensity. It means that tensile stress is increased by increasing the spectrum intensity. This was significant when the spectrum intensity exceeded 40 cm/sec, a value close to the limit suggested in the Japanese guideline for designing gas supply network sensors. From a comparison between shallow and deep burial depths, it is found that deep give a higher tensile stress. Examples of distribution of tensile stress in pipelines walls and along its reinforcement have been shown in **Figure 6.7**. As observed, a condition according to Eurocode 8, with a spectrum intensity value equal to 39 cm/sec, gives higher tensile stress for concrete and reinforcement, with values of 4.5 MPa and 17.3 MPa, respectively. These values are 120% and 3% of the maximum tensile strength of concrete and maximum yielding stress of the steel, respectively, which would correspond to concrete failure in this case. As shown in **Figure 5.11,** the maximum tensile stresses are concentrated at the crown-invert of the inner surface and at the outer surface close to centreline of the cross-section.

Table 7.2: Maximum tensile stress induced in concrete pipelines (Paper II).

Burial depth	Ring stress, MPa			
	Sweden (Se)	Eurocode8 (Eu)	Duzce (Du)	Northridge (NP)
Shallow burial depth	0.56	1.03	0.57	2.32
Deep burial depth	1.87	4.50	2.05	16.10

In Paper III the effect of burial depth, soil layer thickness and non-uniform ground caused by inclined bedrock is studied. The models are subjected to the Swedish design earthquake with high-frequency content and the Chi-Chi earthquake with low-frequency content, see Table 7.3. The results show that with a decrease in burial depth and soil layer thickness, axial stress is decreased. The lowest axial tensile stress appears for models with 12 m soil layer thickness. For axial tensile stress induced by the Swedish design earthquake, the highest maximum axial stress for all types of soils calculated with the model with inclined bedrock, values for dense, medium dense and loose soils reaches 650 kPa, 520 kPa and 230 kPa, respectively. Unlike in the case with the uniformly deep ground, the results show two stress peaks close to the pipe ends, see **Figure 6.13(a)** The peaks for the case with inclined bedrock is concentrated at the centre of the pipe which is situated at the inclined part of the bedrock, see **Figure 6.13(b)**. For axial stresses induced by the Chi-Chi earthquake, all soil types gave a tensile stress equal to 3 MPa, but not for identical geometries. For dense and medium dense soils, this stress level appears in models with 25 m soil layer thickness and 5 m burial depth, while for the case with loose soil it occurs in the case with inclined bedrock.

For tensile bending stresses induced by the Swedish design earthquake, pipelines buried in ground with varying thickness show higher tensile bending stress with all stress peaks towards the right part of pipe, see **Figure 6.13(d)**, whereas for uniformly deep ground, concentration of stresses appears close to the pipe ends, see **Figure 6.13(c)**. Maximum bending stress for dense, medium dense and loose soil is 700 kPa, 560 kPa and 320 kPa, respectively, whereas other models give maximum tensile stresses that are not higher than 220 kPa. For dense and medium dense soils, decreasing soil layer thickness leads to higher bending stresses. For loose soil, increasing the burial depth causes higher bending stresses. For tensile bending stress induced by the Chi-Chi earthquake, the maximum tensile stress for all types of soils occurs for the ground with varying thickness with values of 5.6 MPa, 4.9 MPa and 4.0 MPa for dense, loose and medium dense soils, respectively. For loose and medium dense soils, increasing burial depth gives higher bending stress while decreasing

soil layer thickness leads to lower bending stress. Dense soil and a shallow burial depth in a deep soil layer results in higher stresses.

For ring stresses induced by the Swedish design earthquake, maximum tensile stresses occur in the deeply buried pipelines, with values of 170 kPa, 150 kPa and 65 kPa for dense, medium dense and loose soils, respectively. Soil layer thickness has little effect for dense and medium dense soils but for loose soil smaller thickness gives higher ring stresses. For ring stresses due to the Chi-Chi earthquake, maximum tensile stresses occur for deeply buried pipelines, with values of 500 kPa, 200 kPa and 220 kPa for loose, medium dense and dense soil, respectively. Soil layer thickness has little effect on the ring stresses.

Table 7.3: Maximum tensile stress induced in concrete pipelines (Paper III).

parameter		Axial stress, kPa		Bending stress, kPa		Ring stress, kPa	
		Sweden	Chi-Chi	Sweden	Chi-Chi	Sweden	Chi-Chi
Loose soil	W=25, H=1	78	1147	94	2000	11	63
	W=25, H=5	88	1032	135	2700	65	500
	W=12, H=1	55	552	127	1350	34	66
	α=45°	230	2941	320	4300	-	-
	α=90°	219	3000	320	4900	-	-
Medium soil	W=25, H=1	166	1498	141	1100	56	46
	W=25, H=5	276	2939	100	1300	150	200
	W=12, H=1	167	788	219	800	57	64
	α=45°	617	1892	500	4000	-	-
	α=90°	650	1892	560	4000	-	-
Dense soil	W=25, H=1	302	1975	166	4600	54	78
	W=25, H=5	495	3167	91	1050	170	220
	W=12, H=1	252	1031	218	1200	57	73
	α=45°	520	2342	700	5480	-	-
	α=90°	520	2218	600	5600	-	-

In order to investigate the effect of the piping material, flexible steel pipelines have been chosen for a comparison with rigid concrete pipelines. Analyses for the steel pipelines have been done using a model with 25 m soil layer thickness and 1m burial depth, subjected to the Swedish design earthquake and the Chi-Chi earthquake, see Table 7.4. For axial tensile stresses induced by the Swedish design earthquake and the Chi-Chi earthquake, the maximum stress occurs for dense soil, with values of 2.4 MPa and 14 MPa, respectively.

For bending stresses induced by the Swedish design earthquake medium soil has higher bending stress equal to 640 kPa. For the Chi-Chi earthquake, loose soil has a higher bending stress equal to 11 MPa. Maximum ring tensile stress induced by the Swedish design earthquake and the Chi-Chi earthquake is 10 kPa and 52 kPa, respectively. These maximum stresses are much lower than the maximum axial and bending tensile stresses, but also much lower than the yield stress of the steel.

Maximum tensile stress in steel pipelines occurs for axial stresses induced by the Chi-Chi earthquake with a value of 14 MPa, which is 3 % of the yield strength of steel. In contrast, for comparable concrete pipelines under identical conditions, the maximum tensile stress is 4.5 MPa which exceeds the maximum tensile strength of the concrete. Therefore, the vulnerability of concrete pipelines is much higher than for steel pipelines under these conditions.

Table 7.4: Maximum tensile stress induced in steel pipelines.

Soil type	Axial stress, MPa		Bending stress, MPa		Ring stress, kPa	
	Sweden	Chi-Chi	Sweden	Chi-Chi	Sweden	Chi-Chi
Loose soil	1.0	13.0	0.6	11.0	4	40
Medium soil	1.5	12.5	0.6	6.4	6	52
Dense soil	2.4	14.0	0.5	5.0	10	26

7.2 General conclusions

Two-dimensional finite element models have been developed for simulating propagation of seismic waves from the bedrock through the soil, using Abaqus/Standard. This method enables details of soil geometries to be included and is suitable for the case with high-frequency earthquake loads. Soil-pipe interaction has been considered by non-linear spring

elements to account for slippage at the pipe-soil interface. It was found that infinite elements perform well in representing soil continuity.

The goal of the thesis was to identify parameters that have significant effect on the response of concrete pipelines due to high-frequency earthquake excitations. In this regard, the ground motion input with high-frequency content was introduced at the base of the models where the bedrock is located. Lower frequency content earthquakes with scaled peak acceleration equal to the peak acceleration of high-frequency ground motion input were employed to gain an understanding for the effect of frequency content. The results showed that the response of pipelines due to low-frequency content earthquakes is higher than for high-frequency ones. The main reason is related to the dominant frequency span of the models which were lower or higher than the dominant frequencies of the high-frequency earthquake. But this earthquake affected models with higher frequency content which for dense soil and model with inclined bedrock was significant, whereas low frequency earthquakes had significant effect on models with low frequency content such as loose soil and larger soil layer thickness. It was also concluded that peak acceleration does not represent the severity of earthquakes on buried pipelines. Spectrum intensity was concluded to be a good choice for a pipelines damage indicator.

A study of the parameters related to the soil-pipeline systems showed that critical stress conditions existed for pipelines in non-uniform ground. The concentration of maximum tensile stresses for uniform ground occurred close to the pipelines ends, whereas for non-uniform ground these appeared at the centre and right parts of the pipelines, corresponding to the inclined part and sections with thicker soil layers. In most cases, water mass small effect but was seen to increase bending stresses. Burial depth had significant effect on ring stresses of the pipelines where deeper pipelines showed higher stress. Soil layer thickness had a notable effect on bending stresses induced by high-frequency ground motions. A comparative study between concrete pipelines and steel pipelines indicated high vulnerability for the concrete pipelines. Brittle behaviour of concrete pipelines is especially common in bending, whereas steel pipelines are more flexible in bending but with large axial stresses due to the lower cross-section area.

The presented examples shows, that for the conditions studied, there is less risk for damage on concrete pipelines from high-frequency seismic excitation compared to from earthquakes with lower dominating frequencies. For the three soil types considered the safety from high-frequency damage due to pipe bending was over ten times with respect to the concrete tensile strength. However, this was drastically reduced for cases with varying soil depth due to an inclined bedrock. A major conclusion is that seismic analysis is motivated also for pipelines in high-frequency earthquake areas since local variation in the ground conditions can reduce the safety margin with respect to concrete cracking. In combination with mechanical components of inferior quality, such as pipe joints, this can be a cause for unexpected pipeline failure.

7.3 Future research

The results discussed in this thesis deal with pipelines with joint strengths equal to the pipelines barrel. For future work, the pipelines joints with especial focus on FE models should be investigated. In addition, a study of the effect from the trench surrounding a pipeline is suggested. Furthermore, by defining nonlinear behaviour of the soil, the accuracy of the FE models could be expected to be significantly improved. Studies with focus on comparison between cohesion soils and frictional soils will be performed. Seismic response of pipelines will be studied using models with more than one soil layer in both the vertical and the horizontal direction. The analyses were here performed for a fixed pipe dimension and it is recommended to also investigate the effect of different diameters on the ring stress. Based on the results discussed in this work and by considering the significant effect from non-uniform ground due to inclined bedrock, it can be highly motivated to further study this effect through comparisons of more examples with non-uniform ground, such as rock outcrop.

References

References that only occur in Papers I-III and not in the main text are marked with an asterisk followed by the papers roman numerals.

1. Abaqus 6.12 Online documentation, Dassault Systèmes Simulia Corp. Providence, RI, USA.

2. Ahmed, L., Models for analysis of young cast and sprayed concrete subjected to impact-type loads. Stockholm: KTH Royal Institute of Technology, 2015.

3. American Lifelines Alliance (ALA), Buried Steel Pipes. American Society of Civil Engineers (ASCE) & Federal Emergency Management Agency (FEMA), 2001.

4. American Water Works Association (AWWA), Description of Concrete Pressure Pipe, Concrete Pressure Pipe - Manual of Water Supply Practices, M9 (3rd Edition).

5. American Water Works Association (AWWA), Manufacture and Testing, Steel Pipe - A Guide for Design and Installation - Manual of Water Supply Practices, M11 (4th Edition).

6. Ando, H., Sato, S. and Takagi, N., Seismic observation of a pipeline buried at the heterogeneous ground. Proceedings of the Tenth World Conference on Earthquake Engineering, Balkema, Rotterdam, 1992: p. 5563-5567.*III

7. Arias, A., A measure of earthquake intensity, Seismic designs for nuclear power plants. MIT Press, Cambridge MA, 1970.

8. Arnaout, S. A Comparison Between Bar-Wrapped Concrete Cylinder Pipe and Mortar Lined and Mortar Coated Steel Pipe. Pipeline Division Specialty Conference 2005, Houston, Texas, United States.

9. Bazyar Mansoor Khani, M.H., Dynamic soil-structure interaction analysis using the scaled boundary Finite-Element Method. University of New South Wales: Sydney, 2007.

10. Beieler, R.W., Welded Steel Pipe, Pipelines for Water Conveyance and Drainage. American Society of Civil Engineers (ASCE).

11. Bodare, A. and Kulhanek, O., Dam Safety – Earthquake hazard for dams in Sweden. Elforsk: Stockholm, 2006

12. Bowles, J.E., “Foundation analysis and design”, The McGraw-Hill Companies, NY, 1996. *I, III

13. Bödvarsson, R., Lund, B., Roberts, R., Slunga, R., Earthquake activity in Sweden Study in connection with a proposed nuclear waste repository in Forsmark or Oskarshamn. 2006.

14. Chen, Y., Simplified and refined earthquake analyses for buried pipes. Mathematical and Computer Modelling, 1995. 21(11): p. 47-60.

15. Chopra, A.K., Dynamics of structures, Theory and applications to earthquake engineering. Berkley, Prentice-Hall, Inc., 2001.

16. Chung, D.H., Bernreuter, D.L., The Effect of Regional Variation of Seismic Wave Attenuation on the Strong Ground Motion from Earthquakes. U.S. Nuclear Regulatory Commission, 1981.

17. Das, B.M., Ramana, G.V., “Principles of Soil Dynamic”, 2ed, USA, Cengage Learning, 2011.*I

18. Datta, T.K., Mashaly, E.A., Pipeline response to random ground motion by discrete model. International journal of Earthquake Engineering and Structural Dynamics, 1986. 14: p. 559–572.

19. Datta, T.K., Mashaly, E.A., Seismic response of buried submarine pipelines. Transactions of the ASME, Journal of Energy Resources Technology, 1988: p. 208–218.

20. Datta, T.K., Seismology, Seismic Analysis of Structures. John Wiley & Sons, Ltd., 2010.

21. Datta. S. K, .O'Leary. P.M, Shah, A. H., Three-dimensional dynamic response of buried pipelines to incident longitudinal and shear waves. Journal of Applied Mechanics, 1985. 52(919): p. 915-926.

22. Davis, C. and Bardet, J., Seismic Analysis of Large-Diameter Flexible Underground Pipes. Journal of Geotechnical and Geoenvironmental Engineering, 1998. 124(10): p. 1005-1015.

23. Deeks, A.J., Randolph, M. F., Axisymmetric time-domain transmitting boundaries. Journal of Engineering Mechanics, ASCE, 1994. 120(1): p. 25－42.

24. Dowrick, D., The Nature of Earthquakes, Earthquake Resistant Design and Risk Reduction. John Wiley & Sons, Ltd., 2009.

25. Drivas, G.V., Cost evaluation of seismic load resisting systems based on the ductility classes in Eurocode 8, Master Thesis, KTH Civil and Architectural Engineering, Stockholm, 2014.*I

26. Eguchi, R., Early post-earthquake damage detection for underground lifelines. Final Report to the National Science Foundation, Dames and Moore P.C., Los Angeles, 1991.

27. Eidinger. J.M., Avila. E.A., Reston, Va., Guidelines for the seismic evaluation and upgrade of water transmission facilities. Monograph (American Society of Civil Engineers. Technical Council on Lifeline Earthquake Engineering); American Society of Civil Engineers, 1999.

28. Eurocode 2, "Design of concrete structures, European Standard EN 1992-1-1. European Committee for Standardisation (CEN), Brussels, 2004.[*I]

29. Eurocode 8, Design of structures for earthquake resistance, Part 4: Soils, tanks and pipelines. May 2006.

30. European Standard, Joints for the connection of steel tubes and fittings for water and other aqueous liquids. British Standards Institution (BS EN 10311), 2005.

31. European Standard, Prestressed concrete pressure pipes, cylinder and non-cylinder, including joints, fittings and specific requirement for prestressing steel for pipes. British Standards Institution (BS EN 642:1995), 1995.

32. European Standard, Reinforced concrete pressure pipes, cylinder type, including joints and fittings. British Standards Institution (BS EN 641), 1995.

33. European Standard, Seamless and welded steel tubes. Dimensions and masses per unit length. British Standards Institution (BS EN 10220), 2002.

34. European Standard, Seamless steel tubes for pressure purposes. Technical delivery conditions. British Standards Institution (BS EN 10216), 2002.

35. FEMA: HAZUS-MH MR4, Multi-hazard loss estimation methodology, earthquake model, Technical Manual. National Institute of Building Science: Washington, D.C., 2003.

36. Fukuyama, E., Madariaga, R., Dynamic Rupture Front Interaction on 3D Planar Fault. National Institute for Earth Sciences and Disaster Prevention, Tsukuta, Japan, 1999.

37. Glisic, B., Sensing solutions for assessing and monitoring pipeline systems, Sensor Technologies for Civil Infrastructures, Woodhead Publishing, 2014.

38. Hall, L., Simulations and analyses of train-induced ground vibrations; a comparative study of two- and three-dimensional calculations with actual measurements, Department of Civil and Environmental Engineering. Royal Institute of Technology: Stockholm, Sweden, 2000.

39. Hashash, Y. M. A., Hook, J. J., Schmidt, B., Yao, J. I. C., Seismic design and analysis of underground structures. Tunnelling and Underground Space Technology, 2001. 16(4): p. 247-293.

40. Hellgren, R., Inuence of Fluid Structure Interaction on a Concrete Dam during Seismic Excitation. KTH Royal Institute of Technology: Stockholm, Sweden, 2014.

41. Hindy, A., Novak, M., Earthquake response of underground pipelines. International journal of Earthquake Engineering and Structural Dynamics, 1979, 7: p. 451–476.

42. Hindy, A., Novak, M., Pipeline response to random ground motion. Journal of the Engineering Mechanics Division, 1980. 106: p. 339–360.

43. Hosseini, M., Jalili, S., Azizpour, O., Alikhani, M. Evaluating the functionality of water distribution networks in the aftermath of big earthquakes based on nonlinear modeling of pipes connections. ASCE Pipeline Conference. 2010, Kingston. Colorado, USA.

44. Hosseini, M., Roudsari, M.T. A study on the effect of surface transverse waves on buried steelpipelines considering the nonlinear behaviour of soil and pipes. ASCE Pipeline Conference. 2010, Kingston, Colorado, USA.

45. Housner, G.W., Intensity of ground motion during strong earthquakes, in A technical report on research conducted under contract with the office of Naval research. California Institute of Technology, 1952.

46. Hovland, T.J. and M. Najafi, 10. Steel Pipe, Inspecting Pipeline Installation. American Society of Civil Engineers (ASCE).

47. Ichimura, T., Fujita, K., Hori, M., Sakanoue, T., Hamanaka, R., Three-Dimensional Nonlinear Seismic Ground Response Analysis of Local Site Effects for Estimating Seismic Behavior of Buried Pipelines. Journal of Pressure Vessel Technology-Transactions of the Asme, 2014. 136(4).*III

48. IITK-GSDMA, Guidelines for Seismic Design of Buried Pipelines. November 2007.

49. Katayama, T., Kubo, K., and Sito, N. . Earthquake damage to water and gas distribution systems. Proceedings of the US National Conference on Earthquake Engineering, EERI, Ann Arbor, MI. 1975.

50. Kouretzis, G.P., Bouckovalas, G.D, Gantes, C.J., 3-D shell analysis of cylindrical underground structures under seismic shear (S) wave action. Soil Dynamic Earthquake Engineering, 2006. 26: p. 909-921.

51. Kouretzis, G.P., Bouckovalas, G.D., Karamitros, D.K., Seismic verification of long cylindrical underground structures considering Rayleigh wave effects. Tunnelling and Underground Space Technology, 2011. 26: p. 789-794.

52. Kramer, S.L., Geotechnical earthquake engineering. Prentice-Hall, Upper Saddle River, NJ., 1996.

53. Kubo, K. Behaviour of underground water pipes during earthqauke. in 5th word conference on earthquake enginearing. 1973. Rome.

54. Lanzano, G., Salzano, E., Santucci De Magistris, F., Fabbrocino, G., An observational analysis of seismic vulnerability of industrial pipelines. Chemical Engineering Transaction, 2012. 26: p. 567-572.

55. Lanzano, G., Santucci De Magistris, F., Fabbrocino, G., Salzano, E., Integrated approach to the seismic vulnerability assessment of industrial underground equipment and pipelines. Bollettino di Geofisica Teorica ed Applicata, 2014. 55(1): p. 215-226.

56. Lee, D.H., Kim, B.H., Lee, H., Kong, J.S., Seismic behaviour of a buried gas pipeline under earthquake excitations. Journal of Engineering Structures, 2009. 31: p. 1011–1023.

57. Liang, J.W. and S.P. Sun, Site effects on seismic behaviour of pipelines: A review. Journal of Pressure Vessel Technology-Transactions of the Asme, 2000. 122(4): p. 469-475.*III

58. Liu, J.B and Du, Y.X., 3D spring-viscous artificial boundary in time domain. Earthquake Engineering and Engineering Vibration, 2006. 5(1): p. 93-102.

59. Lysmer, J., Kulemeyer, R. L., Finite dynamic model for infinite media. Journal of Engineering Mechanics, ASCE, 1969. 95: p. 759－877.

60. McGuire, R. K. and Hanks, T. C. , RMS Acceleration and spectral amplitudes of strong ground motion during the San Fernando, CA, earthquake. Bultin of Seismological Society of America, 1980. 70(5): p. 1907-1970.

61. Mewmark, N.M., Problems in wave propagation in soil and rock. Proc. Int. Symposium on Wave Propagation and Dynamic Properties of Earth Materials, Albuquerque, New Mexico, 1967, 7-26.

62. Meyer, P., The Impact of High Frequency/Low Energy Seismic Waves on Unreinforced Masonry. Massachusetts Institute of Technology, 2006.

63. Moser, A.P., Buried Pipe Design. The McGraw-Hill Companies, 2001.

64. Muleski, G.E., Ariman, T., Aumen, C.P., A shell model for buried pipes in earthquakes. Journal of soil dynamics and earthquake engineering, 1985. 4: p. 43–51.

65. Nakayama, W., Shimizu, Y., Koganemaru, K., Development of super dense real-time disaster mitigation system for urban gas supply network. Journal of Japan Association for Earthquake Engineering, 2004: p. 124-127.

66. Novak, M., Hindy, A., Seismic analysis of underground tubular structures. Proceeding of the Seventh World Conference Earthquake Engineering, 1980. 8: p. 287–294.

67. O'Rourke, M.J., Liu X., Response of buried pipelines subjected to earthquake effects. MCEER , University of New York, Buffalo, USA, 1999.

68. O'Rourke, M. and G. Ayala, Pipeline damage due to wave-propagation. Journal of Geotechnical Engineering-Asce, 1993. 119(9): p. 1490-1498.* III

69. O'Rourke, M.J., Castro, G., Effects of seismic wave propagation upon buried pipelines. Earthquake Engineering and Structural Dynamics, 1980. 8: p. 455-467.

70. Owen, G.N., Scholl, R.E, Earthquake engineering of large underground structures. Washington, D.C, USA: Federal Highway Administration and National Science Foundation, 1981.

71. (PEER), Pacific Earthquake Engineering Research Center, http://peer.berkeley.edu/. 2014.

72. Pineda-Porras, O. and Ordaz, M., A new seismic intensity parameter to estimate damage in buried pipelines due to seismic wave propagation. Journal of Earthquake Engineering, 2007. 11(5): p. 773-786.

73. Pineda-Porras, O. and Ordaz, M., Seismic Damage Estimation in Buried Pipelines Due to Future Earthquakes - The Case of the Mexico City Water System. Intech., 2012.

74. Pineda-Porras, O. and Ordaz, M., Seismic Damage Estimation in Buried Pipelines Due to Future Earthquakes – The Case of the Mexico City Water System, Earthquake-Resistant Structures: Design, Assessment And Rehabilitation, Intech, 2012.

75. Pineda-Porras, O. and Ordaz-Schroeder, M., Seismic Vulnerability Function for High-Diameter Buried Pipelines: Mexico City's Primary Water System Case. ASCE International Conference on Pipeline Engineering and Construction. 2003.

76. Ratnayaka, D.D., Brandt, M.J., and Johnson, M.K., Water Supply (6th Edition), Elsevier, 2009.

77. Roudsari, M.T., Hosseini, M., Using neural network for reliability assessment of buried steel pipeline networks subjected to earthquake wave propagation. Journal of Applied Sciences, 2011. 11(18): p. 3233-3246.

78. Rydell, C., Seismic high-frequency content loads on structures and components within nuclear facilities, Civil and Architectural Engineering. KTH Stockholm, 2014.

79. S:T Eriks, Underground Infrastructures, Handbook for water and waste water networks, 2013 (in Swedish).

80. Saberi, M., Behnamfar, F., Vafaeian, M., A semi-analytical model for estimating seismic behavior of buried steel pipes at bend point under propagating waves. Bulletin of Earthquake Engineering Journal, 2013. 11: p. 1373–1402.

81. Sadat Shokouhi, S.K., Dolatshah, A., Vosoughifar, H.R., Hosseininejad, S.Z., Rahnavard, Y. Optimal sensor placement of TYTON joints in the water pipeline networks Subjected to near-fault and far-fault earthquakes. Proceedings of the Pipelines Conference. Fort Worth, 2013, Texas.

82. Sadat Shokouhi, S.K., Mokhlespour, M.E. Optimal sensor placement for bolted-gland joints in the water pipeline networks subjected to near-fault and far-fault earthquakes. International Conf on Pipelines and Trenchless Technology. Xi'an, China, 2013.

83. Seismosoft, http://www.seismosoft.com/en/SeismoSignal.aspx, 2014.[*I]

84. Seismosoft. http://www.seismosoft.com/en/SeismoMatch.aspx. 2014.

85. (SKI), Seismic safety –Characterization of seismic ground motions for probabilistic safety analyses of nuclear facilities in Sweden. Swedish Nuclear Power Inspectorate (SKI): Stockholm, 1992.

86. Tabatabei-Araghi, P., Seismic analysis of concrete structures within nuclear industry, in KTH Royal Institute of Technology (SE). 2014.

87. Takada, S., N. Hassani, and K. Fukuda, Damage directivity in buried pipelines of Kobe City during the 1995 earthquake. Journal of Earthquake Engineering, 2002. 6(1): p. 1-15.[*III]

88. Takada, S., Tanabe, K., Three dimensional seismic response analysis of buried continuous or jointed pipelines. Pressure Vessel Techn., ASME, 1987. 109: p. 80–87.

89. Tromans, I., Behaviour of buried water supply pipelines in earthquake zones, in Department of Civil and Environmental Engineering. University of London, 2004.

90. Vassilev, V.H., Flores-Berrones, R., Seismic analysis of segmented buried pipelines. Proceeding of Eleventh World Conference on Earthquake Engineering, 1986.

91. Wang, L.R.L., Cheng, K. M., Seismic Response Behavior of Buried Pipelines. Journal of Pressure Vessel Technology, 1979. 101(1): p. 21-30.

92 www.wikipedia.org/wiki/Nyquist_rate

93. Xu, L., Ye, Z. C., Ren, Q. W., Zhang, L., FEM Analysis of Dynamic Response of Buried Fiber Reinforced Plastic Matrix Pipe under Seismic Load. Mathematical Problems in Engineering, 2013.

94. Yang, R., Kameda, H., Takada, S., Shell model FEM analysis of buried pipelines under seismic loading. Bull. Disas. Prey. Res. Inst., Kyoto Univ., 1988. 38(336): p. 115-146.

95. Yeh, G.C.K., Seismic analysis of slender buried beams. Bulletin of the Seismological Society of America, 1974. 64(5): p. 1551-1562.

96. Zienkiewicz, O.C., Emson, C., and Bettess, P., A Novel Boundary Infinite Element. International Journal for Numerical Methods in Engineering, 1983. 19: p. 393–404.